

Review

Model-based transmission line fault location methods: A review

Yu Liu^{a,b,*}, Dayou Lu^a, Stepan Vasilev^c, Binglin Wang^a, Dian Lu^a, Vladimir Terzija^c^a School of Information Science and Technology, ShanghaiTech University, Shanghai 201210, China^b Key Laboratory of Control of Power Transmission and Conversion (SJTU), Ministry of Education, Shanghai 200240, China^c Center for Energy Science and Technology, Skolkovo Institute of Science and Technology, Moscow 121205, Russia

ARTICLE INFO

Keywords:

Distributed parameters
 Fault location
 Model-based method
 Phasor domain
 Time domain
 Transmission line

ABSTRACT

Accurate fault location methods for transmission lines are essential to ensure secure and reliable operation of power systems. Among various fault location approaches, model-based fault location methods are widely adopted in practical power systems since they are compatible with typical data acquisition systems and have clear physical meanings. There are extensive phasor domain and time domain model-based approaches in the existing literature, however, the connections among various line models, as well as corresponding fault location approaches, are not fully investigated. To this end, this paper first systematically reviews transmission line modeling framework for fault location, including time domain and phasor domain matrix/scalar form lumped/distributed parameter models. The relationships between these models are carefully presented and discussed, with clear assumptions for each model. Next, different phasor domain and time domain model-based fault location methods using various line models are shown in detail. Finally, numerical experiments verify the differences between different model-based methods and the importance to use accurate line models for transmission line fault location. The results also clearly indicate the advantages of time domain model-based methods over phasor domain methods: the time domain approaches can accurately locate faults using a short data window within half a cycle after the fault occurs. Compared to traveling wave based methods, the time domain model-based methods are compatible with available data acquisition hardware in substations, with a relatively low sampling rates of several kilo-samples/sec.

1. Introduction

Power transmission lines are critically important components of power systems, transmitting large quantity of power over long distances. Modern power systems usually include both AC and DC transmission lines [1–2]. With increasing penetration of renewables in future power grids, reliable operations of transmission lines are essential to ensure safe and secure energy transmission from renewables to customers. However, faults often occur on transmission lines. After the faulted transmission line is selectively isolated from the rest of the power system, accurate fault location schemes are valuable to minimize the time spent searching for the fault, reduce the power outage time and improve power supply quality and reliability [3–5]. Taking overhead lines as examples, the fault usually occurs at the tower or between two towers, which means that the fault location can be determined by finding the towers near the line fault [78–79]. In practical application, the accuracy of the fault location method is required to be within a few percent of the line length (such as less than 1% of the length) for different fault types

and fault resistances [80]. There are extensive number of fault location methods in the existing literatures. They can be mainly classified into traveling wave based methods, data driven methods, and model-based methods.

Traveling wave based methods [6–10] locate faults by detecting the arrival time of wavefronts at terminals of the line. They can be further classified into type A, C, E, F methods (single-ended) and type B, D (dual-ended) methods [6]. The limitations of traveling wave based methods are as follows. For AC transmission lines, first, the intensity of traveling waves generated by the fault is affected by the fault initiation time and the fault resistance; the wavefront may not be reliably detected if the fault inception angle is close to zero or during high resistance faults. Second, traveling wave could also be generated by events in the system other than line internal faults, which may affect the detection of first or subsequent wavefronts. Third, since the speed of traveling waves is close to the speed of light, traveling wave based methods typically require very high sampling rates (with the order of MHz) to ensure high time resolution and fault location accuracy. However, such data acquisition

* Corresponding author.

E-mail addresses: liuyu.shanghaitech@gmail.com, liuyu@shanghaitech.edu.cn (Y. Liu).<https://doi.org/10.1016/j.ijepes.2023.109321>

Received 28 December 2022; Received in revised form 21 April 2023; Accepted 16 June 2023

Available online 26 June 2023

0142-0615/© 2023 Elsevier Ltd. All rights reserved.

systems with very high sampling rates may not be available in practice AC system. For HVDC transmission lines, traveling wave based fault location devices with the sampling frequency of several MHz have been applied to practical power systems. For HVDC lines, the intensity of traveling waves will not be affected by the fault inception time since the pre-fault waveforms are almost DC. However, wavefront detection for DC faults could still be challenging during high resistance faults, and location accuracy is still dependent on the accurate detection of first or subsequent wavefronts. To ensure accuracy, very high sampling rate (with the order of MHz) is similarly required, which is not typically available in DC substations.

Data driven methods [11–18] (also known as artificial intelligence based methods, or machine learning based methods) locate faults through extraction of information from a large set of data. Various data driven based tools, including k -nearest neighbour (kNN) [11], support vector machine (SVM) [12], decision tree (DT) [13], neural network (NN) [14], convolutional neural network (CNN) [15], graph neural network (GNN) [16], etc., are adopted for fault location. There are also data driven methods that consider the inherent physical laws of the fault location problem (physics informed data driven methods), to further improve the performance of fault location [17–18]. The primary challenge of data driven methods is the availability of high-quality training data that can cover different scenarios of faults, including various fault types, inception angles, fault resistances, fault locations, and system operating conditions. As a result, there are very limited applications of data driven fault location methods in practical power systems.

The most widely adopted fault location methods in practical power systems are the model-based methods. In practical power systems, transmission lines are generally equipped with phasor measurements from protective relays or from phasor measurement units (PMUs). In addition, for digital substations, instantaneous sampled value (SV) measurements are available from merging units (MUs), with typical sampling rate of 4000 or 4800 samples/sec (80 samples/cycle for 50 or 60 Hz systems) according to IEC 61850-9-2 standard [19]. Moreover, transmission lines are also generally equipped with digital fault recorders (DFRs) to record instantaneous voltages and currents during faults; the recorded waveforms are stored in COMTRADE files [20] with the typical sampling rate of several to tens of kilo-samples/second as well. Phasor and time domain model-based fault location approaches are quite compatible with the available data acquisition hardware (phasors from relays or PMUs, instantaneous measurements from MUs or DFRs, etc.) in practical substations, and have clear physical meanings. The key idea of model-based fault location methods is to build accurate transmission line models that describe physical laws of the transmission line with fault, and then solve for the fault location. With the increasing penetration of renewables in future power systems, transmission lines are experiencing more severe and unusual transients during faults. In this case, line models that can accurately describe the physical relationship between transmission line voltages and currents during faults are essential to ensure fault location accuracy.

According to detailed domain of the line model, model-based fault location methods can be further classified into phasor domain and time domain methods. Phasor domain model-based fault location methods [6,21–30] assume sinusoidal steady state operation of the AC power systems, and utilize voltage and current fundamental frequency phasors (complex numbers) to represent sinusoidal waveforms. Among phasor domain fault location methods, the utilized phasor domain line models include lumped RL models [6], lumped π models [21–24] and fully distributed parameter models [25–30]. Typically, accurate extraction of phasors from instantaneous voltage and current waveforms are required [31–33]. With phasor representations, the phasor domain fault location problem typically solves algebraic equations, simplifying the fault location procedure. However, due to the steady state assumptions, phasor domain methods will generate fault location errors for systems during severe transients (e.g. the available time window during faults are very short, even less than 1 cycle) or without fundamental

frequencies (eg. DC transmission lines). In these cases, time domain methods can be applied. Time domain model-based fault location methods [34–44] directly describes the time domain physical laws of the transmission line with fault, without sinusoidal steady state assumptions. Therefore, time domain methods are compatible with short fault data window and fault location problems in DC transmission lines. Among time domain fault location methods, the utilized time domain line models include lumped RL models [34], lumped single/multi-section π models [35–37], Bergeron models [38–41], and fully distributed parameter models [42–44], to name a few. However, as time domain line models are usually represented via ordinary differential equations or even partial differential equations, the time domain fault location procedures are generally more complicated than phasor domain approaches. On the other hand, they are also not sensitive to decaying DC component existing in fault currents, as well as they are not sensitive to signal distortions [63–68].

Although model-based fault location methods have been presented in many literatures, there are still several important questions to be answered, as follows. First, among all those phasor and time domain transmission line models utilized for fault location, what are the connections between them, and how to evaluate the accuracy of each model? Second, how to use these transmission line models to formulate model-based fault location methods? Third, what is the impact of different transmission line models on the fault location accuracy? To this end, this paper systematically summarizes various time domain and phasor domain transmission line models for fault location, presents the assumption of each model, and establishes the logic flow among those models. Afterwards, the paper introduces different types of model-based fault location approaches with reference to various transmission line models. Finally, numerical experiments compare the performances of different phasor domain and time domain model-based fault location methods, where the impact of line modeling accuracy is carefully evaluated, and the applicability of different methods is also demonstrated.

The rest of the paper is organized as follows. Section 2 systematically summarizes modeling aspects of transmission lines, including various transmission line models. Section 3 presents details of model-based fault location methods, with different transmission line models. Section 4 shows numerical experimental results for comparative study. Section 5 makes further discussions. Section 6 draws conclusions.

2. Transmission line modeling

In this part, the transmission line modeling procedure for fault location is thoroughly reviewed. Transmission line models can be extremely complex, and therefore the solutions of those models are challenging. To simplify the solution procedure, researchers proposed models that are with certain assumptions. Nevertheless, more assumptions usually result in more errors in transmission line models and therefore inaccurate transmission line fault location results. The overall transmission line modeling procedure for fault location is depicted in Fig. 1. Part 2.1 introduces the most accurate transmission line model, which is hard to solve. Part 2.2 to 2.5 derive different line models in time domain, while Part 2.6 to 2.9 derive different line models in phasor domain, with certain assumptions for each model. Note that the transmission line modeling procedure in this part is applicable to not only overhead transmission lines but also underground cables. However, the shunt capacitances per unit length of underground cables are much larger, and the frequency dependent characteristics of underground cables are much more influential than those of the overhead lines.

For AC and DC lines, the different modeling procedures could be considered. Note that the line models in time domain are based on the voltage and current waveforms directly, and are suitable for both AC and DC transmission lines. Therefore, the line models in Part 2.1 to Part 2.5 are applicable for both AC and DC lines. In Part 2.6 to 2.9, the line models in phasor domain are based on the voltage and current fundamental phasor measurements, which are only available for AC lines.

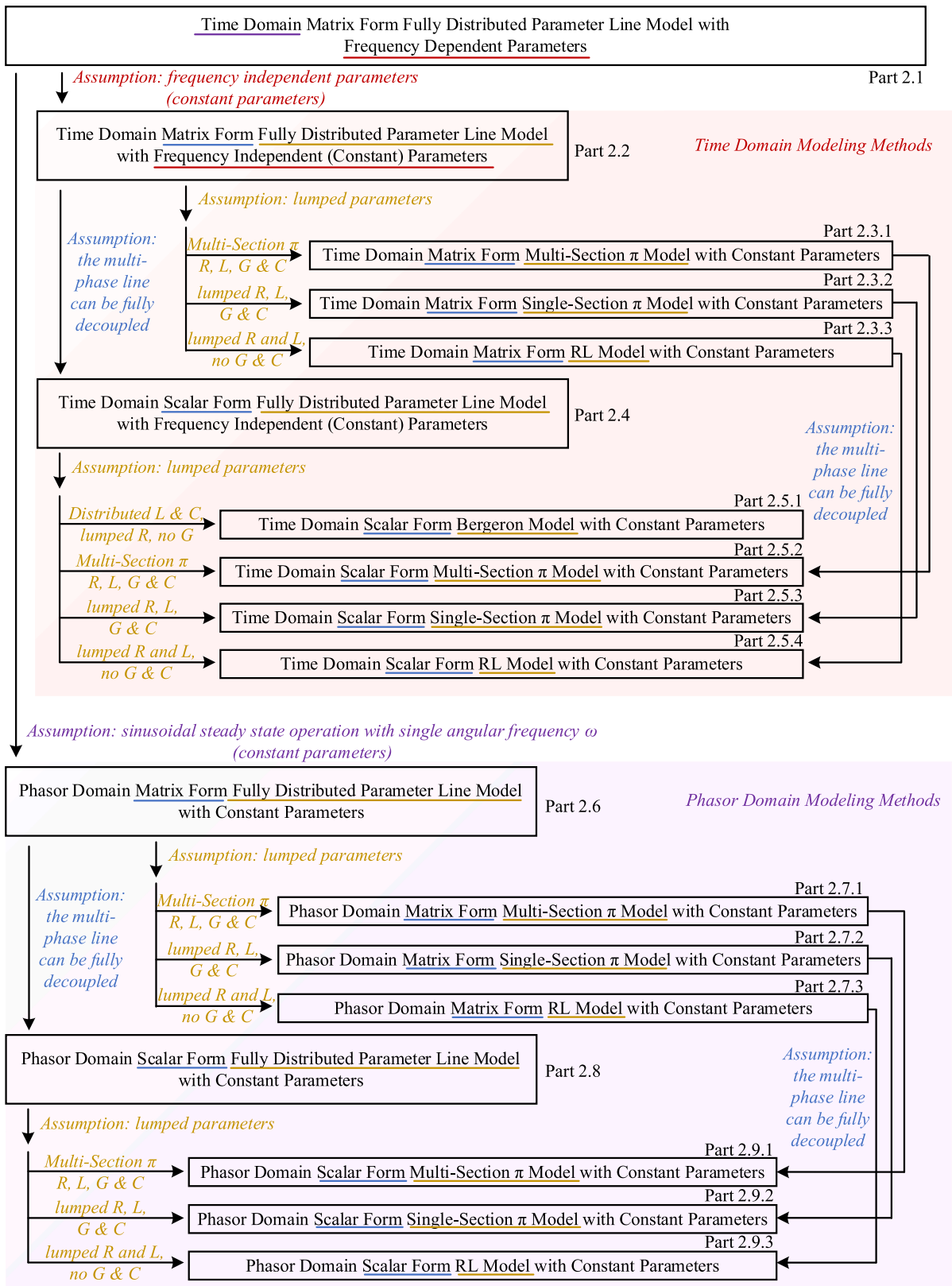


Fig. 1. Overall transmission line modeling procedure for fault location.

Therefore, the line models in phasor domain are usually adopted for AC lines. In addition, the fault location methods according to those phasor domain and time domain line models are carefully designed, which are provided in Part 3.

2.1. Time domain matrix form fully distributed parameter line model with frequency dependent parameters

The most accurate transmission line model is the time domain, matrix form, fully distributed parameter transmission line model with

frequency dependent parameters. The equivalent circuit of an example multi-phase transmission line is shown in Fig. 2, where the phase number is n . Typically, the phase number is 3 for a three-phase AC transmission line, and the phase (pole) number is 2 for a two-pole DC transmission line. In addition, the mutually coupled transmission circuits on the same tower or sharing the same right-of-way can also be represented as a multi-phase line model. For example, a double-circuit AC transmission line sharing the same tower corresponds to a multi-phase line model with $n = 6$.

The transmission line is with the length of l . The terminal current and voltage vectors at the sending end and the receiving end are $\mathbf{i}_S(t)$, $\mathbf{i}_R(t)$, $\mathbf{u}_S(t)$, and $\mathbf{u}_R(t)$, respectively. To model the transmission line with fully distributed parameters, the line is separated into infinite number of sections, where each section is with the infinitesimal length of dx . The example section with length dx at location x is shown in the figure. The series resistance matrix, series inductance matrix, shunt conductance matrix and shunt capacitance matrix per unit length are $\mathbf{R}(x,t)$, $\mathbf{L}(x,t)$, $\mathbf{G}(x,t)$ and $\mathbf{C}(x,t)$, respectively. Note that since the transmission line is with frequency dependent parameters, those matrices are not constant and are represented by functions of location x and time t . Here, the time domain line model is based on the voltage and current waveforms. At different distance x and time t , the frequency components of waveforms are usually different. Due to the frequency dependent characteristic, to be general, the line parameters are described as functions of x and t .

From Fig. 2, for each infinitesimal section dx , one can write (a) the Kirchhoff's Current Laws (KCL) at the left terminal of this section and (b) the Kirchhoff's Voltage Laws (KVL) between the left and the right side of the section. Those result in equations in (1).

$$\begin{aligned} \mathbf{i}(x+dx, t) &= \mathbf{i}(x, t) + \mathbf{G}(x, t)dx \cdot \mathbf{u}(x, t) + \mathbf{C}(x, t)dx \cdot \frac{\partial \mathbf{u}(x, t)}{\partial t} \\ \mathbf{u}(x+dx, t) &= \mathbf{u}(x, t) + \mathbf{R}(x, t)dx \cdot \mathbf{i}(x, t) + \mathbf{L}(x, t)dx \cdot \frac{\partial \mathbf{i}(x, t)}{\partial t} \end{aligned} \quad (1)$$

After reorganizing (1) and letting $dx \rightarrow 0$, the following equation can be obtained,

$$\begin{cases} \frac{\partial \mathbf{u}(x, t)}{\partial x} + \mathbf{L}(x, t) \frac{\partial \mathbf{i}(x, t)}{\partial t} + \mathbf{R}(x, t) \mathbf{i}(x, t) = \mathbf{0} \\ \frac{\partial \mathbf{i}(x, t)}{\partial x} + \mathbf{C}(x, t) \frac{\partial \mathbf{u}(x, t)}{\partial t} + \mathbf{G}(x, t) \mathbf{u}(x, t) = \mathbf{0} \end{cases} \quad (2)$$

Equation (2) is the general format of the time domain matrix form fully distributed parameter line model with frequency dependent parameters. In fact, one can observe that equation (2) is a set of matrix form partial differential equations (PDEs) with time-varying coefficient. This equation is difficult to solve for fault location application. Therefore, assumptions are made to simplify this model.

Next, time domain simplifications are introduced in part 2.2 to 2.5, while phasor domain simplifications are introduced in part 2.6 to 2.9. For all the following line models, the three-phase AC transmission line is

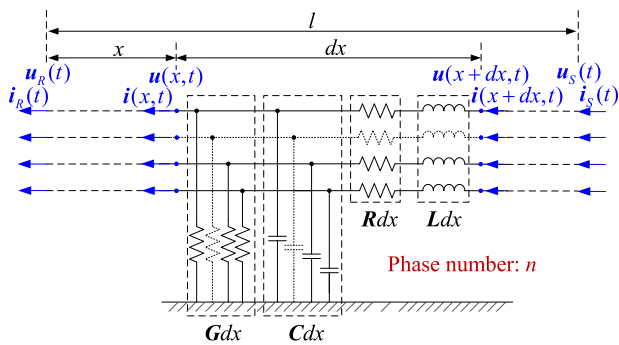


Fig. 2. Equivalent circuit, time domain matrix form fully distributed parameter line model with frequency dependent parameters, multi-phase line with phase number n .

adopted as an example. For time domain line models in part 2.2 to 2.5, the modeling procedure can be similarly applied to general AC or DC lines with different number of phases or poles. For phasor domain models in part 2.6 to 2.9, the models are applicable to general AC lines with different number of phases.

2.2. Time domain matrix form fully distributed parameter line model with frequency independent (constant) parameters

The first assumption that can simplify the model in (2) is to assume frequency independent parameters. The line model is shown Fig. 3. With this assumption, the transmission line model is [43],

$$\begin{cases} \frac{\partial \mathbf{u}(x, t)}{\partial x} + \mathbf{L} \frac{\partial \mathbf{i}(x, t)}{\partial t} + \mathbf{R} \mathbf{i}(x, t) = \mathbf{0} \\ \frac{\partial \mathbf{i}(x, t)}{\partial x} + \mathbf{C} \frac{\partial \mathbf{u}(x, t)}{\partial t} + \mathbf{G} \mathbf{u}(x, t) = \mathbf{0} \end{cases} \quad (3)$$

where \mathbf{R} , \mathbf{L} , \mathbf{G} and \mathbf{C} are constant series resistance matrix, series inductance matrix, shunt conductance matrix and shunt capacitance matrix per unit length.

Equation (3) is the general format of the time domain matrix form fully distributed parameter line model with frequency independent parameters. This equation is a matrix form PDE with constant parameters, and can be solved using numerical solution of matrix form PDE [43]. However, this matrix form PDE is still challenging to solve, and is without analytical solutions.

To further simplify (3), there are mainly two ways. The first way is to introduce matrix form lumped parameter models (in part 2.3). The second way is to decouple the matrix form PDE into scalar form PDEs (in part 2.4) and afterwards introduce scalar form lumped parameter models (in part 2.5).

2.3. Time domain matrix form lumped parameter model with constant parameters

In this part, the time domain lumped parameter models in matrix form are introduced. The lumped parameter models may include the multi-section π model, the single-section π model, and the RL model.

2.3.1. Time domain matrix form multi-section π model with constant parameters

The key idea of multi-section models is to use finite number of sections (with section number n) to closely approximate the line model in Fig. 3 with infinite number of sections. The accuracy of this approximation is high with large section numbers. This idea is shown in Fig. 4. For each section, the line model is chosen as the π model. The definitions of parameters are the same as Fig. 3. For each section k ($k = 1, 2, \dots, n$), the terminal current and voltage vectors at the left end and the right end are $\mathbf{i}_{k, \text{left}}(t)$, $\mathbf{i}_{k, \text{right}}(t)$, $\mathbf{u}_{k, \text{left}}(t)$, and $\mathbf{u}_{k, \text{right}}(t)$, respectively; the inductor current vector is $\mathbf{i}_{Lk}(t)$. The physical laws that section k ($k = 1, 2, \dots, n$) should obey include [35–36],

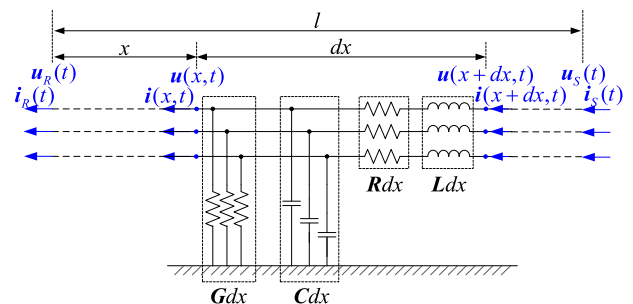


Fig. 3. Equivalent circuit, time domain matrix form fully distributed parameter line model with frequency independent (constant) parameters.

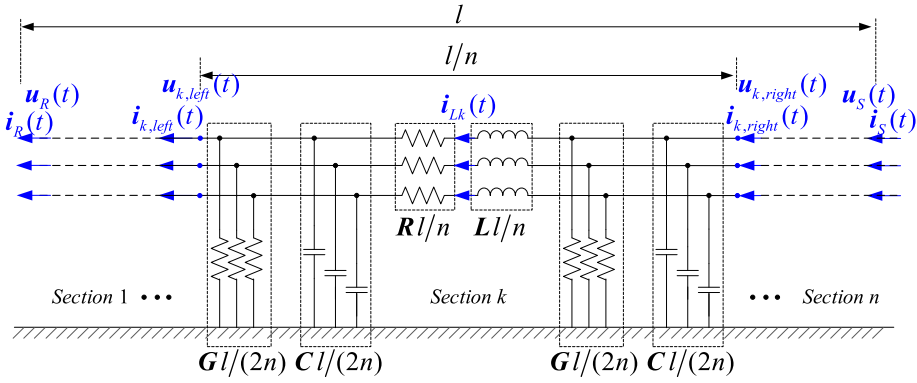


Fig. 4. Equivalent circuit, time domain matrix form multi-section π model with constant parameters.

$$\begin{cases} \mathbf{i}_{k, \text{left}}(t) = -\frac{Gl}{2n} \mathbf{u}_{k, \text{left}}(t) - \frac{Cl}{2n} \frac{d\mathbf{u}_{k, \text{left}}(t)}{dt} + \mathbf{i}_{Lk}(t) \\ \mathbf{i}_{k, \text{right}}(t) = \frac{Gl}{2n} \mathbf{u}_{k, \text{right}}(t) + \frac{Cl}{2n} \frac{d\mathbf{u}_{k, \text{right}}(t)}{dt} + \mathbf{i}_{Lk}(t) \\ \mathbf{0} = -\mathbf{u}_{k, \text{right}}(t) + \mathbf{u}_{k, \text{left}}(t) + \frac{Rl}{n} \mathbf{i}_{Lk}(t) + \frac{Ll}{n} \frac{d\mathbf{i}_{Lk}(t)}{dt} \end{cases} \quad (4)$$

Besides, since the two adjacent π sections share the same node, the following equations hold for $k = 1, 2, \dots, n-1$,

$$\begin{cases} \mathbf{i}_{k, \text{right}}(t) = \mathbf{i}_{k+1, \text{left}}(t) \\ \mathbf{u}_{k, \text{right}}(t) = \mathbf{u}_{k+1, \text{left}}(t) \end{cases} \quad (5)$$

Also, the terminal voltages and currents are consistent with the definitions of π sections, i.e.,

$$\begin{cases} \mathbf{i}_{1, \text{left}}(t) = \mathbf{i}_R(t), \quad \mathbf{u}_{1, \text{left}}(t) = \mathbf{u}_R(t) \\ \mathbf{i}_{n, \text{right}}(t) = \mathbf{i}_S(t), \quad \mathbf{u}_{n, \text{right}}(t) = \mathbf{u}_S(t) \end{cases} \quad (6)$$

2.3.2. Time domain matrix form single-section π model with constant parameters

One extreme case of multi-section π model is when the section number n is selected as 1. In this case, the model becomes a single-section π model as shown in Fig. 5. The physical laws of this model can be described as [35–36],

$$\begin{cases} \mathbf{i}_R(t) = -\frac{Gl}{2} \mathbf{u}_R(t) - \frac{Cl}{2} \frac{d\mathbf{u}_R(t)}{dt} + \mathbf{i}_L(t) \\ \mathbf{i}_S(t) = \frac{Gl}{2} \mathbf{u}_S(t) + \frac{Cl}{2} \frac{d\mathbf{u}_S(t)}{dt} + \mathbf{i}_L(t) \\ \mathbf{0} = -\mathbf{u}_S(t) + \mathbf{u}_R(t) + R\mathbf{i}_L(t) + L\frac{d\mathbf{i}_L(t)}{dt} \end{cases} \quad (7)$$

2.3.3. Time domain matrix form RL model with constant parameters

To further simplify the line model, the shunt capacitance and

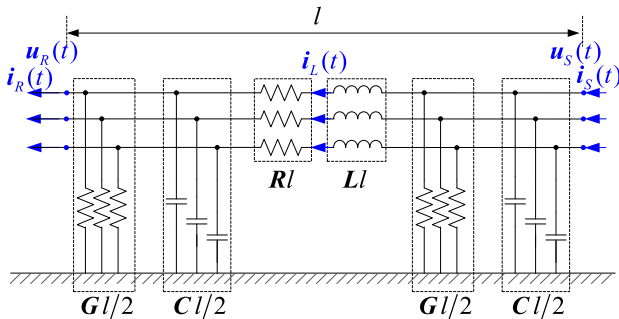


Fig. 5. Equivalent circuit, time domain matrix form single-section π model with constant parameters.

conductance are neglected, resulting in an RL model as shown in Fig. 6. The physical laws of this model can be described as [34],

$$\begin{cases} \mathbf{i}_R(t) = \mathbf{i}_L(t), \quad \mathbf{i}_S(t) = \mathbf{i}_L(t) \\ \mathbf{0} = -\mathbf{u}_S(t) + \mathbf{u}_R(t) + R\mathbf{i}_L(t) + L\frac{d\mathbf{i}_L(t)}{dt} \end{cases} \quad (8)$$

2.4. Time domain scalar form fully distributed parameter line model with constant parameters

One main challenge of solving (3) is that the equations are in the matrix form. For multi-phase transmission lines, since there are non-zero off-diagonal elements in matrices R, L, G and C , the voltages and currents of different phases are coupled together. Therefore, in order to further simplify the line modeling, one can decouple (3) into PDEs of several modes, where the voltages and currents in each mode are independent of those in other modes. This transformation usually has the following form,

$$\begin{cases} \mathbf{u}(x, t) = \mathbf{T}_u \cdot \mathbf{u}_{\text{mode}}(x, t) \\ \mathbf{i}(x, t) = \mathbf{T}_i \cdot \mathbf{i}_{\text{mode}}(x, t) \end{cases} \quad (9)$$

With the transformation in (9), equation (3) can be rewritten as,

$$\begin{cases} \frac{\partial \mathbf{u}_{\text{mode}}(x, t)}{\partial x} + \mathbf{T}_u^{-1} \mathbf{L} \mathbf{T}_i \frac{\partial \mathbf{i}_{\text{mode}}(x, t)}{\partial t} + \mathbf{T}_u^{-1} \mathbf{R} \mathbf{T}_i \mathbf{i}_{\text{mode}}(x, t) = \mathbf{0} \\ \frac{\partial \mathbf{i}_{\text{mode}}(x, t)}{\partial x} + \mathbf{T}_i^{-1} \mathbf{C} \mathbf{T}_u \frac{\partial \mathbf{u}_{\text{mode}}(x, t)}{\partial t} + \mathbf{T}_i^{-1} \mathbf{G} \mathbf{T}_u \mathbf{u}_{\text{mode}}(x, t) = \mathbf{0} \end{cases} \quad (10)$$

For general parameter matrices R, L, G and C , one may not be able to find constant transformation matrices T_u and T_i that can fully decouple the multi-phase transmission line. If the transmission line is geometrically symmetrical, i.e., for each matrix of R, L, G and C , the diagonal elements are the same and the off-diagonal elements are the same, there are many possible selections of T_u and T_i that can fully decouple (3).

Taking three phase transmission line as examples, one can use constant transformations such as Clarke transformation (11) or Karrenbauer transformation (12) for decoupling [45],

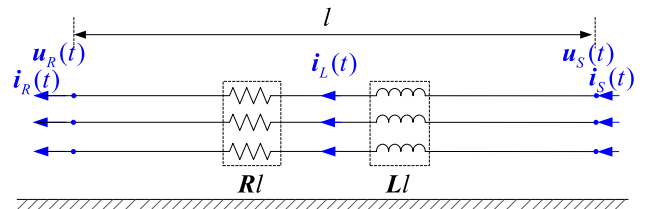


Fig. 6. Equivalent circuit, time domain matrix form RL model with constant parameters.

$$\mathbf{T}^{-1} = \mathbf{T}_u^{-1} = \mathbf{T}_i^{-1} = \frac{1}{3} \begin{bmatrix} 2 & -1 & -1 \\ 0 & \sqrt{3} & -\sqrt{3} \\ 1 & 1 & 1 \end{bmatrix} \quad (11)$$

$$\mathbf{T}^{-1} = \mathbf{T}_u^{-1} = \mathbf{T}_i^{-1} = \frac{1}{3} \begin{bmatrix} 1 & 0 & -1 \\ 0 & 1 & -1 \\ 1 & 1 & 1 \end{bmatrix} \quad (12)$$

In this case, $\mathbf{T}_u^{-1}\mathbf{L}\mathbf{T}$, $\mathbf{T}_u^{-1}\mathbf{R}\mathbf{T}_i$, $\mathbf{T}_i^{-1}\mathbf{C}\mathbf{T}_u$ and $\mathbf{T}_i^{-1}\mathbf{G}\mathbf{T}_u$ are all diagonal matrices, and equation (10) becomes [42],

$$\begin{cases} \frac{\partial u_j(x,t)}{\partial x} + L_j \frac{\partial i_j(x,t)}{\partial t} + R_j i_j(x,t) = 0 \\ \frac{\partial i_j(x,t)}{\partial x} + C_j \frac{\partial u_j(x,t)}{\partial t} + G_j u_j(x,t) = 0 \end{cases} \quad (13)$$

where subscript j corresponds to the mode j after decoupling. One can observe that both sub-equations in (13) are 1-dimensional (scalar form) PDEs and are easier to solve. The line model of mode j is shown in Fig. 7. These 1-dimensional PDEs also enable further simplified modeling for transmission lines, as shown in part 2.5.

2.5. Time domain scalar form lumped parameter model with constant parameters

In this part, the time domain lumped parameter models in scalar form are introduced. The lumped parameter models may include the Bergeron model, the multi-section π model, the single-section π model, and the RL model.

2.5.1. Time domain scalar form Bergeron model with constant parameters

The scalar form equations enable analytical solutions to the PDEs in (13). To find analytical solutions to (13), one way is to neglect the series resistance R_j and shunt conductance G_j , resulting in a lossless fully distributed parameter line model, as shown in (14),

$$\begin{cases} \frac{\partial u_j(x,t)}{\partial x} + L_j \frac{\partial i_j(x,t)}{\partial t} = 0 \\ \frac{\partial i_j(x,t)}{\partial x} + C_j \frac{\partial u_j(x,t)}{\partial t} = 0 \end{cases} \quad (14)$$

The general solution corresponding to (14) can be obtained from d'Alembert formula,

$$i_j(x,t) = f_{j,1}(x-vt) + f_{j,2}(x+vt) \quad (15)$$

$$u_j(x,t) = Z_j f_{j,1}(x-vt) - Z_j f_{j,2}(x+vt) \quad (16)$$

where $f_{j,1}$ and $f_{j,2}$ are two different functions of x and t ; $v = 1/\sqrt{L_j C_j}$ is the speed of traveling waves of mode j , and $Z_j = \sqrt{L_j/C_j}$ is the surge impedance of mode j .

In order to obtain the aforementioned analytical solutions of voltages and currents at mode j , the series resistance R_j and shunt conductance G_j are neglected. This procedure will cause modeling errors. To also consider the effect of series resistance, the Bergeron model separates the mode j resistance of the entire line (namely $R_{total,j}$) into 3 lumped parts:

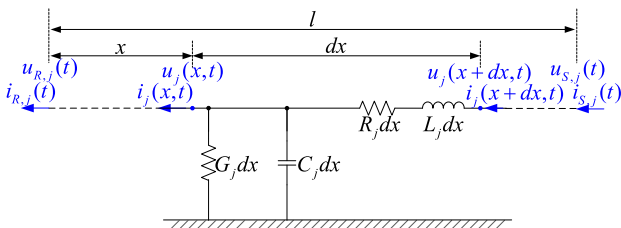


Fig. 7. Equivalent circuit, time domain scalar form fully distributed parameter line model with constant parameters.

$1/4 R_{total,j}$, $1/2 R_{total,j}$, $1/4 R_{total,j}$. The lines between two adjacent lumped resistors are modelled as lossless fully distributed parameter lines, with the length of $l/2$. This procedure is shown in Fig. 8.

From the physical laws, the analytical relationship among terminal voltages and currents of mode j is [38–39],

$$\begin{aligned} i_{R,j}(t) = & 1/Z_j \cdot u_{R,j}(t) - (1+h)/2 \cdot [1/Z_j \cdot u_{R,j}(t-\tau) \\ & + h \cdot i_{R,j}(t-\tau)] - (1-h)/2 \cdot [1/Z_j \cdot u_{S,j}(t-\tau) + h \cdot i_{S,j}(t-\tau)] \end{aligned} \quad (17)$$

Note that the Bergeron model includes of 2 lossless line sections with distributed capacitance and inductance parameters, and 3 lump resistors. To distinguish the Bergeron model from PDE model with fully distributed line parameters (3), here the Bergeron model is presented into the category of “lump parameter models”. Indeed, it can also be classified as a “distributed parameter model”.

2.5.2. Time domain scalar form Multi-Section π model with Constant parameters

Similar as 2.3.1, the multi-section model utilizes finite number of sections (with section number n) to closely approximate the line model in Fig. 7 with infinite number of sections. The accuracy of this approximation is high with large section numbers. This idea is shown in Fig. 9. For each section, the line model is chosen as the π model. The definitions of parameters are exactly the same as those in Fig. 7. For each section k ($k = 1, 2, \dots, n$) and mode j , the terminal current and voltage vectors at the left end and the right end are $\mathbf{i}_{k,left,j}(t)$, $\mathbf{i}_{k,right,j}(t)$, $\mathbf{u}_{k,left,j}(t)$, and $\mathbf{u}_{k,right,j}(t)$, respectively; the inductor current vector is $\mathbf{i}_{Lk,j}(t)$. The physical laws that section k ($k = 1, 2, \dots, n$) should obey include [35–36],

$$\begin{cases} i_{k,left,j}(t) = -\frac{G_j l}{2n} u_{k,left,j}(t) - \frac{C_j l}{2n} \frac{du_{k,left,j}(t)}{dt} + i_{Lk,j}(t) \\ i_{k,right,j}(t) = \frac{G_j l}{2n} u_{k,right,j}(t) + \frac{C_j l}{2n} \frac{du_{k,right,j}(t)}{dt} + i_{Lk,j}(t) \\ 0 = -u_{k,right,j}(t) + u_{k,left,j}(t) + \frac{R_j l}{n} i_{Lk,j}(t) + \frac{L_j l}{n} \frac{di_{Lk,j}(t)}{dt} \end{cases} \quad (18)$$

Besides, since the two adjacent π sections share the same node, the following equations hold for $k = 1, 2, \dots, n-1$,

$$\begin{cases} i_{k,right,j}(t) = i_{k+1,left,j}(t) \\ u_{k,right,j}(t) = u_{k+1,left,j}(t) \end{cases} \quad (19)$$

Also, the terminal voltages and currents are consistent with the definitions of π sections, i.e.,

$$\begin{cases} i_{1,left,j}(t) = i_{R,j}(t), \quad u_{1,left,j}(t) = u_{R,j}(t) \\ i_{n,right,j}(t) = i_{S,j}(t), \quad u_{n,right,j}(t) = u_{S,j}(t) \end{cases} \quad (20)$$

2.5.3. Time domain scalar form single-section π model with constant parameters

Similar as 2.3.2, if we select section number $n = 1$, the model becomes a single-section π Model as shown in Fig. 10. The physical laws of this model can be described as [35–36],

$$\begin{cases} i_{R,j}(t) = -\frac{G_j l}{2} u_{R,j}(t) - \frac{C_j l}{2} \frac{du_{R,j}(t)}{dt} + i_{L,j}(t) \\ i_{S,j}(t) = \frac{G_j l}{2} u_{S,j}(t) + \frac{C_j l}{2} \frac{du_{S,j}(t)}{dt} + i_{L,j}(t) \\ 0 = -u_{S,j}(t) + u_{R,j}(t) + R_j l i_{L,j}(t) + L_j l \frac{di_{L,j}(t)}{dt} \end{cases} \quad (21)$$

2.5.4. Time domain scalar form RL model with constant parameters

Similar as 2.3.3, if the shunt capacitance and conductance are neglected, an RL model is established as shown in Fig. 11. The physical laws of this model can be described as [34],

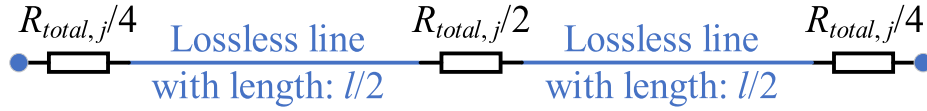


Fig. 8. Equivalent circuit, time domain scalar form Bergeron model with constant parameters.

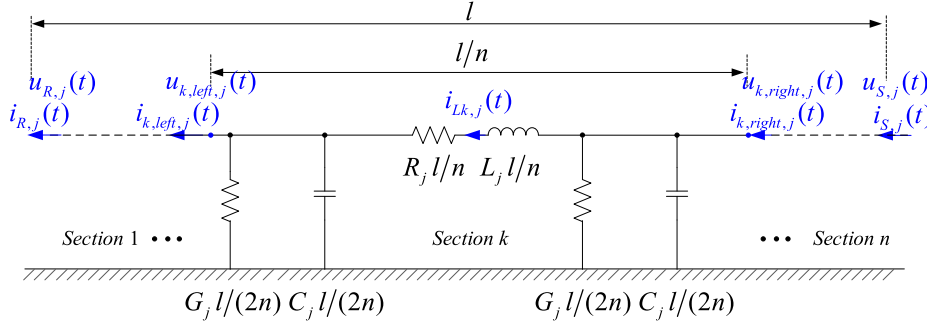


Fig. 9. Equivalent circuit, time domain scalar form multi-section π model with constant parameters.

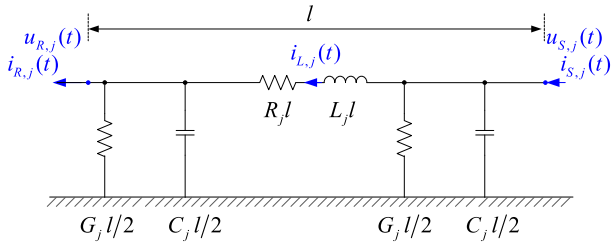


Fig. 10. Equivalent circuit, time domain scalar form single-section π model with constant parameters.

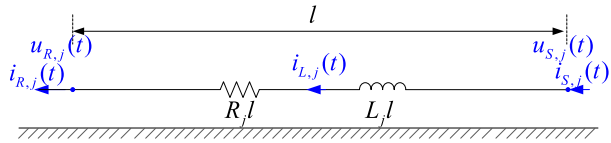


Fig. 11. Equivalent circuit, time domain scalar form RL model with constant parameters.

$$\begin{cases} i_R(t) = i_L(t), & i_S(t) = i_L(t) \\ 0 = -u_S(t) + u_R(t) + R_j i_L(t) + L_j l \frac{di_L(t)}{dt} \end{cases} \quad (22)$$

2.6. Phasor domain matrix form fully distributed parameter line model with constant parameters

Part 2.2 to 2.5 derive the time domain transmission line modeling methods. Next, the phasor domain transmission line modeling methods are derived. Most time domain models do not have analytical solution. On the contrary, phasor domain modeling procedure converts the time domain operators (such as d/dt) into phasor domain operators (such as $j\omega$, where ω is the angular frequency of the system), enabling great simplifications. In general, phasor domain models have analytical solutions. However, phasor domain methods have following assumptions: (a) the system is a linear time-invariant system; (b) the sources of the system are sinusoidal, with unique angular frequency ω ; and (c) the system operates in steady state (no system transients are considered).

With aforementioned assumptions, equation (2) can be further simplified. The line model in Fig. 2 can be converted into phasor domain, as shown in Fig. 12. Note that here the capital letter with tilde is the phasor domain representation of the corresponding lower case variable in time domain (eg. $\tilde{U}(x + dx)$ is the phasor domain representation

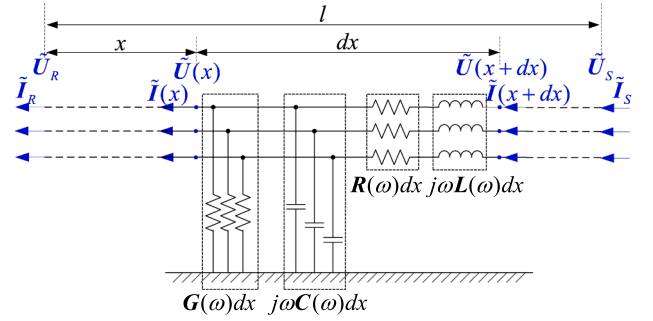


Fig. 12. Equivalent circuit, phasor domain matrix form fully distributed parameter line model with constant parameters.

of $\mathbf{u}(x + dx, t)$ in time domain). Also, here since the angular frequency of the system is fixed as ω , the frequency dependent parameter matrices per unit length become constants: $\mathbf{R}(\omega)$, $\mathbf{L}(\omega)$, $\mathbf{G}(\omega)$ and $\mathbf{C}(\omega)$. For phasor domain transmission line models, in the rest of the paper, the parameter matrices per unit length in phasor domain are represented as \mathbf{R} , \mathbf{L} , \mathbf{G} and \mathbf{C} for simplicity. In this case, the transmission line model in phasor domain can be derived from Fig. 12 (or directly converting (2) into phasor domain) [28],

$$\begin{cases} \frac{d\tilde{\mathbf{U}}(x)}{dx} + (\mathbf{R} + j\omega\mathbf{L})\tilde{\mathbf{I}}(x) = \mathbf{0} \\ \frac{d\tilde{\mathbf{I}}(x)}{dx} + (\mathbf{G} + j\omega\mathbf{C})\tilde{\mathbf{U}}(x) = \mathbf{0} \end{cases} \quad (23)$$

One can observe from (23) that with phasor domain representation, the matrix form PDEs (where x and t are two independent variables) are converted into matrix form ordinary differential equations (ODEs) (where x is the only independent variable). These ODEs can be solved analytically. The solutions indicate the following relationship among terminal voltage and current phasor vectors [28],

$$\begin{bmatrix} \tilde{\mathbf{U}}_S \\ \tilde{\mathbf{I}}_S \end{bmatrix} = \begin{bmatrix} \mathbf{I}_{m \times m} & \mathbf{0} \\ \mathbf{0} & \mathbf{A} \end{bmatrix}^{-1} e^{j\mathbf{B}x} \begin{bmatrix} \mathbf{I}_{m \times m} & \mathbf{0} \\ \mathbf{0} & \mathbf{A} \end{bmatrix} \begin{bmatrix} \tilde{\mathbf{U}}_R \\ \tilde{\mathbf{I}}_R \end{bmatrix} \quad (24)$$

where the definitions are: $\mathbf{A} = \mathbf{R} + j\omega\mathbf{L}$, $\mathbf{B} = (\mathbf{R} + j\omega\mathbf{L})(\mathbf{G} + j\omega\mathbf{C})$; $\mathbf{I}_{m \times m}$ is an identity matrix with the dimension of m , and m is the number of phases of the transmission line. The matrix function $e^{j\mathbf{B}x}$ is defined as $\sum_{n=0}^{\infty} \frac{(j\mathbf{B}x)^n}{n!}$.

2.7. Phasor domain matrix form lumped parameter model with constant parameters

In this part, the phasor domain lumped parameter models in matrix form are introduced. The lumped parameter models may include the multi-section π model, the single-section π model, and the RL model. Note that the corresponding line models are the same as part 2.3 except that these models are in phasor domain.

2.7.1. Phasor domain matrix form multi-section π model with constant parameters

The key idea of multi-section models is to use finite number of sections (with section number n) to closely approximate the line model in Fig. 12 with infinite number of sections. The equivalent circuit is shown in Fig. 13. The definitions of variables and the corresponding physical laws are consistent with those in part 2.3.1. After conversion, the line models in phasor domain are algebraic equations [24],

$$\begin{cases} \tilde{\mathbf{I}}_{k,\text{left}} = -\frac{(\mathbf{G} + j\omega\mathbf{C})l}{2n}\tilde{\mathbf{U}}_{k,\text{left}} + \tilde{\mathbf{I}}_{Lk} \\ \tilde{\mathbf{I}}_{k,\text{right}} = \frac{(\mathbf{G} + j\omega\mathbf{C})l}{2n}\tilde{\mathbf{U}}_{k,\text{right}} + \tilde{\mathbf{I}}_{Lk} \quad (\text{for } k = 1, 2, \dots, n) \\ \mathbf{0} = -\tilde{\mathbf{U}}_{k,\text{right}} + \tilde{\mathbf{U}}_{k,\text{left}} + \frac{(\mathbf{R} + j\omega\mathbf{L})l}{n}\tilde{\mathbf{I}}_{Lk} \end{cases} \quad (25)$$

$$\begin{cases} \tilde{\mathbf{I}}_{k,\text{right}} = \tilde{\mathbf{I}}_{k+1,\text{left}} \quad (\text{for } k = 1, 2, \dots, n-1) \\ \tilde{\mathbf{U}}_{k,\text{right}} = \tilde{\mathbf{U}}_{k+1,\text{left}} \end{cases} \quad (26)$$

$$\begin{cases} \tilde{\mathbf{I}}_{1,\text{left}} = \tilde{\mathbf{I}}_R, \quad \tilde{\mathbf{U}}_{1,\text{left}} = \tilde{\mathbf{U}}_R \\ \tilde{\mathbf{I}}_{n,\text{right}} = \tilde{\mathbf{I}}_S, \quad \tilde{\mathbf{U}}_{n,\text{right}} = \tilde{\mathbf{U}}_S \end{cases} \quad (27)$$

2.7.2. Phasor domain matrix form single-section π model with constant parameters

The matrix form single-section π model in phasor domain is shown in Fig. 14. The physical laws of this model can be described as [24],

$$\begin{cases} \tilde{\mathbf{I}}_R = -\frac{(\mathbf{G} + j\omega\mathbf{C})l}{2}\tilde{\mathbf{U}}_R + \tilde{\mathbf{I}}_L \\ \tilde{\mathbf{I}}_S = \frac{(\mathbf{G} + j\omega\mathbf{C})l}{2}\tilde{\mathbf{U}}_S + \tilde{\mathbf{I}}_L \\ \mathbf{0} = -\tilde{\mathbf{U}}_S + \tilde{\mathbf{U}}_R + (\mathbf{R} + j\omega\mathbf{L})\tilde{\mathbf{I}}_L \end{cases} \quad (28)$$

2.7.3. Phasor domain matrix form RL model with constant parameters

The matrix form RL model in phasor domain is shown in Fig. 15. The physical laws of this model can be described as [6],

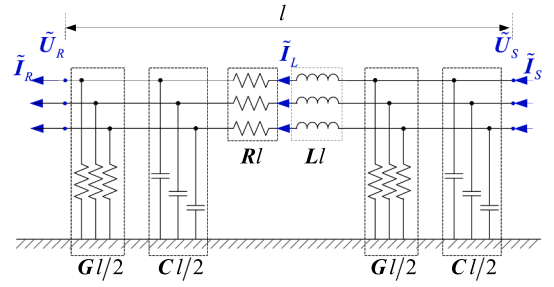


Fig. 14. Equivalent circuit, phasor domain matrix form single-section π model with constant parameters.

$$\begin{cases} \tilde{\mathbf{I}}_R = \tilde{\mathbf{I}}_L, \quad \tilde{\mathbf{I}}_S = \tilde{\mathbf{I}}_L \\ \mathbf{0} = -\tilde{\mathbf{U}}_S + \tilde{\mathbf{U}}_R + (\mathbf{R} + j\omega\mathbf{L})\tilde{\mathbf{I}}_L \end{cases} \quad (29)$$

2.8. Phasor domain scalar form fully distributed parameter line model with constant parameters

Another way of solving (23) is to convert the matrix form ODEs into scalar form (1-dimensional) ODEs. For multi-phase transmission lines, since there are non-zero off-diagonal elements in matrices \mathbf{R} , \mathbf{L} , \mathbf{G} and \mathbf{C} , the voltages and currents of different phases are coupled together. Therefore, in order to further simplify the line modeling, one can decouple (23) into ODEs of several modes, where the voltages and currents in each mode are independent of those in other modes. This transformation usually have the following form,

$$\begin{cases} \tilde{\mathbf{U}}(x) = \mathbf{T}_u \cdot \tilde{\mathbf{U}}_{\text{mode}}(x) \\ \tilde{\mathbf{I}}(x) = \mathbf{T}_i \cdot \tilde{\mathbf{I}}_{\text{mode}}(x) \end{cases} \quad (30)$$

With the transformation in (30), equation (23) can be rewritten as,

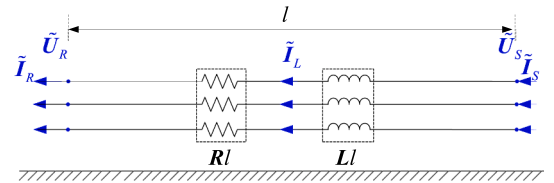


Fig. 15. Equivalent circuit, phasor domain matrix form RL model with constant parameters.

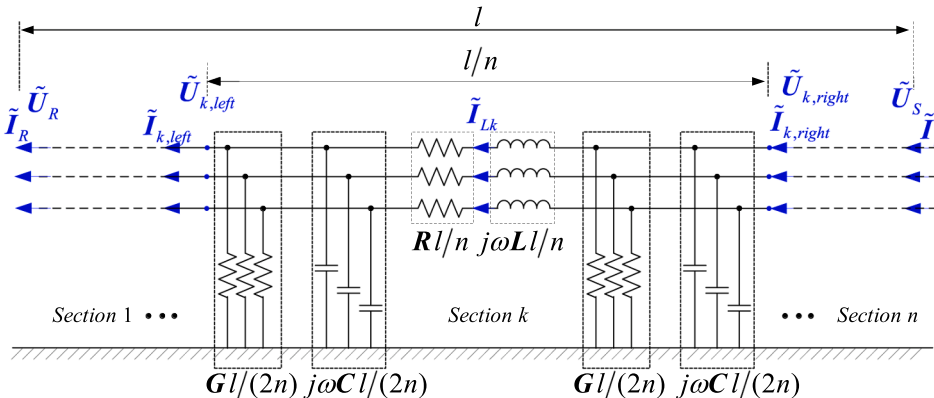


Fig. 13. Equivalent circuit, phasor domain matrix form multi-section π model with constant parameters.

$$\begin{cases} \frac{d\tilde{\mathbf{U}}_{mode}(x)}{dx} + \mathbf{T}_u^{-1}(\mathbf{R} + j\omega\mathbf{L})\mathbf{T}_i \cdot \tilde{\mathbf{I}}_{mode}(x) = \mathbf{0} \\ \frac{d\tilde{\mathbf{I}}_{mode}(x)}{dx} + \mathbf{T}_i^{-1}(\mathbf{G} + j\omega\mathbf{C})\mathbf{T}_u \cdot \tilde{\mathbf{U}}_{mode}(x) = \mathbf{0} \end{cases} \quad (31)$$

Specifically, if the transmission line is geometrically symmetrical, i. e., for each matrix of \mathbf{R} , \mathbf{L} , \mathbf{G} and \mathbf{C} , the diagonal elements are the same and the off-diagonal elements are the same. In this case, similar as part 2.4, the transformations such as Clarke transformation (11) or Karrenbauer transformation (12) can also be utilized for decoupling. In addition, for phasor domain models, the symmetrical component transformation (32) is also widely adopted [45].

$$\mathbf{T}^{-1} = \mathbf{T}_u^{-1} = \mathbf{T}_i^{-1} = \frac{1}{3} \begin{bmatrix} 1 & e^{j120^\circ} & e^{-j120^\circ} \\ 1 & e^{-j120^\circ} & e^{j120^\circ} \\ 1 & 1 & 1 \end{bmatrix} \quad (32)$$

In this case, $\mathbf{T}_u^{-1}\mathbf{L}\mathbf{T}_u$, $\mathbf{T}_u^{-1}\mathbf{R}\mathbf{T}_u$, $\mathbf{T}_i^{-1}\mathbf{C}\mathbf{T}_u$ and $\mathbf{T}_i^{-1}\mathbf{G}\mathbf{T}_u$ are all diagonal matrices, and equation (31) becomes,

$$\begin{cases} \frac{d\tilde{U}_j(x)}{dx} + (R_j + j\omega L_j) \cdot \tilde{I}_j(x) = 0 \\ \frac{d\tilde{I}_j(x)}{dx} + (G_j + j\omega C_j) \cdot \tilde{U}_j(x) = 0 \end{cases} \quad (33)$$

where subscript j corresponds to the mode j after decoupling. One can observe that both sub-equations in (13) are 1-dimensional (scalar form) ODEs and are easier to solve. The line model of mode j is shown in Fig. 16. These ODEs can be directly solved. The solutions indicate the following relationship among terminal voltage and current phasor vectors for mode j [25],

$$\begin{bmatrix} \tilde{V}_{S,j} \\ \tilde{I}_{S,j} \end{bmatrix} = \begin{bmatrix} \cosh(p_j l) & Z_j \sinh(p_j l) \\ \frac{1}{Z_j} \sinh(p_j l) & \cosh(p_j l) \end{bmatrix} \begin{bmatrix} \tilde{V}_{R,j} \\ \tilde{I}_{R,j} \end{bmatrix} \quad (34)$$

where $Z_j = \sqrt{(R_j + j\omega L_j)/(G_j + j\omega C_j)}$, $p_j = \sqrt{(R_j + j\omega L_j)(G_j + j\omega C_j)}$.

2.9. Phasor domain scalar form lumped parameter model with constant parameters

In this part, the phasor domain lumped parameter models in scalar form are introduced. The phasor domain lumped parameter models may also include the multi-section π model, the single-section π model, and the RL model. Note that the scalar form fully distributed line parameter model in PDE form can be directly simplified into ODE form, which can be directly solved analytically as (34). Therefore, the ‘‘phasor domain version’’ of the ‘‘Bergeron model (lumped resistors and distributed inductance/capacitance) is not included here.

2.9.1. Phasor domain scalar form multi-section π model with constant parameters

Similar as 2.7.1, the key idea of multi-section models is to use finite

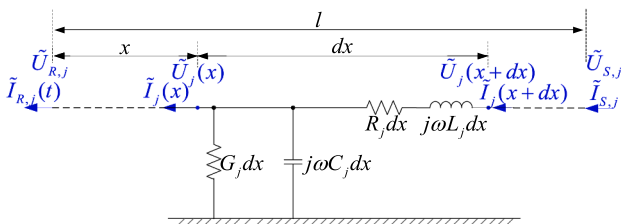


Fig. 16. Equivalent circuit, phasor domain scalar form fully distributed parameter line model with constant parameters.

number of sections (with section number n) to closely approximate the line model in Fig. 16 with infinite number of sections. The equivalent circuit is shown in Fig. 17. After conversion, the line models in phasor domain are algebraic equations [24],

$$\begin{cases} \tilde{I}_{k,left,j} = -\frac{(G_j + j\omega C_j)l}{2n} \tilde{U}_{k,left,j} + \tilde{I}_{Lk,j} \\ \tilde{I}_{k,right,j} = \frac{(G_j + j\omega C_j)l}{2n} \tilde{U}_{k,right,j} + \tilde{I}_{Lk,j} \quad (for\ k = 1, 2, \dots, n) \\ 0 = -\tilde{U}_{k,right,j} + \tilde{U}_{k,left,j} + \frac{(R_j + j\omega L_j)l}{n} \tilde{I}_{Lk,j} \end{cases} \quad (35)$$

$$\begin{cases} \tilde{I}_{k,right,j} = \tilde{I}_{k+1,left,j} \quad (for\ k = 1, 2, \dots, n-1) \\ \tilde{U}_{k,right,j} = \tilde{U}_{k+1,left,j} \end{cases} \quad (36)$$

$$\begin{cases} \tilde{I}_{1,left,j} = \tilde{I}_{R,j}, \quad \tilde{U}_{1,left,j} = \tilde{U}_{R,j} \\ \tilde{I}_{n,right,j} = \tilde{I}_{S,j}, \quad \tilde{U}_{n,right,j} = \tilde{U}_{S,j} \end{cases} \quad (37)$$

2.9.2. Phasor domain scalar form single-section π model with constant parameters

Similar as 2.7.2, the scalar form single-section π model in phasor domain is shown in Fig. 18. The physical laws of this model can be described as [24],

$$\begin{cases} \tilde{I}_{R,j} = -\frac{(G_j + j\omega C_j)l}{2} \tilde{U}_{R,j} + \tilde{I}_{L,j} \\ \tilde{I}_{S,j} = \frac{(G_j + j\omega C_j)l}{2} \tilde{U}_{S,j} + \tilde{I}_{L,j} \\ 0 = -\tilde{U}_{S,j} + \tilde{U}_{R,j} + (R_j + j\omega L_j) \tilde{I}_{L,j} \end{cases} \quad (38)$$

2.9.3. Phasor domain scalar form RL model with constant parameters

Similar as 2.7.3, the scalar form RL model in phasor domain is shown in Fig. 19. The physical laws of this model can be described as [6],

$$\begin{cases} \tilde{I}_{R,j} = \tilde{I}_{L,j}, \quad \tilde{I}_{S,j} = \tilde{I}_{L,j} \\ 0 = -\tilde{U}_{S,j} + \tilde{U}_{R,j} + (R_j + j\omega L_j) \tilde{I}_{L,j} \end{cases} \quad (39)$$

3. Model-based fault location methods

In this part, the fault location methods based on the line models in part 2 are presented. Phasor domain methods utilize voltage and current phasor measurements, which can be accurately extracted during sinusoidal steady state for AC transmission lines. Typically, the best performance of the phasor domain methods requires a relatively long data window after the fault occurs. For the cases during severe transients (such as the available time window during faults are too short to extract accurate phasors) or when the fault occurs in DC lines (without fundamental frequencies), the performances of phasor domain methods will be compromised. For these cases, the time domain methods are

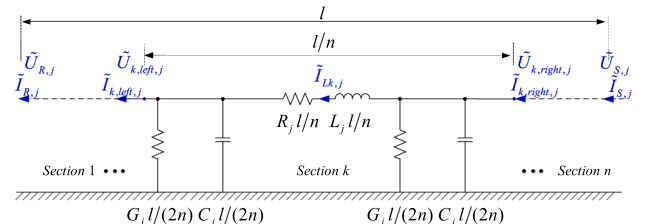


Fig. 17. Equivalent circuit, time domain scalar form multi-section π model with constant parameters.

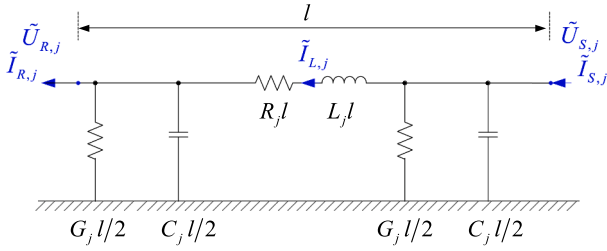


Fig. 18. Equivalent circuit, phasor domain scalar form single-section π model with constant parameters.

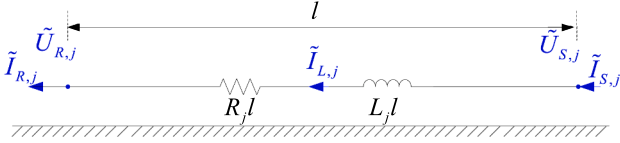


Fig. 19. Equivalent circuit, phasor domain scalar form RL model with constant parameters.

compatible with sampled-value instantaneous measurements within a short time window. It is worth noting that time domain methods can also work for the cases with accurate phasor measurements. However, in those cases, time domain methods are not preferred, because the phasor domain methods are usually more simplified than time domain methods.

3.1. Phasor domain methods

Phasor domain methods are based on phasor domain models from Section 2.6–2.9.

3.1.1. Single-ended phasor domain method

In this part, the single-ended phasor domain method is introduced. The most widely adopted method is the impedance based method (also known as the simple reactance method) [6]. The line is modelled as the phasor domain scalar form RL model with constant parameters (with the model in 2.9.3). The fault location algorithm measures the imaginary part of the apparent line impedance seen at the local terminal. The location is obtained as the following equation [6],

$$l_f = \frac{\text{Im}(\tilde{V}/\tilde{I})}{\text{Im}(Z_{1L})} \quad (40)$$

where \tilde{V} and \tilde{I} are calculated according to the local three phase voltage and current measurements, which is shown in the Table 1. Z_{1L} and Z_{0L} are the positive (negative) and zero sequence impedance of the per unit length line, $k_0 = (Z_{0L} - Z_{1L})/Z_{1L}$ is the zero-sequence compensation factor.

In fact, the previous single-ended method assumes that the fault resistance is zero. If the fault resistance is considered, the previous expression may encounter errors. The key challenge is how to eliminate the impact of fault resistance. There are also a number of methods with improvements, such as those assuming homogeneity of source impedance and line impedance (eg. Takagi methods) [46–48], or assuming known source impedance at the remote terminal of the line (eg. Eriksson methods) [48–49]. There are also some other additional single-ended methods, which are based on different phasor models of the transmission line [50].

3.1.2. Dual-ended phasor domain method

In this part, the dual-ended phasor domain method is introduced. Usually, different line models can be adopted in the dual-ended phasor domain method. The key idea is that the voltage at the fault location can either be calculated from the left side or the right side of the line ter-

minal. In this case, the effect of fault resistance can be well eliminated. The general fault location procedure can be summarized as follows. Note that the models in 2.6–2.9 can be generally represented as the two-port network as [28],

$$\begin{bmatrix} \tilde{\mathbf{U}}_S \\ \tilde{\mathbf{I}}_S \end{bmatrix} = \mathbf{A}(l) \begin{bmatrix} \tilde{\mathbf{U}}_R \\ \tilde{\mathbf{I}}_R \end{bmatrix} \quad (41)$$

where $\mathbf{A}(l)$ is a coefficient matrix of the line model with the length l . For the matrix form model, $\tilde{\mathbf{U}}_S, \tilde{\mathbf{U}}_R, \tilde{\mathbf{I}}_S, \tilde{\mathbf{I}}_R$ are three phase voltages and currents at the sending (“S”) and the receiving (“R”) ends, respectively, and $\mathbf{A}(l)$ can be calculated according to the model with line parameters matrix. For the scalar form model, $\tilde{U}_S, \tilde{U}_R, \tilde{I}_S, \tilde{I}_R$ are three mode voltages and currents, and $\mathbf{A}(l)$ can be calculated by combining three independent scalar form model with mode parameters.

The fault model can also be adopted to improve the redundancy of the fault location problem. The fault model can be represented as,

$$\mathbf{0}_{3 \times 1} = \tilde{\mathbf{I}}_{f1} + \tilde{\mathbf{I}}_{f2} - \mathbf{M}_{fault} \tilde{\mathbf{U}}_f \quad (42)$$

where the matrix \mathbf{M}_{fault} is defined in Table 2, and Y_f is the fault admittance.

During the fault, the transmission line can be divided into three parts: the left section, the right section and the fault model, as shown in Fig. 20. The left section and the right section can be represented as the two-port networks. The left section can be generally represented as,

$$\begin{bmatrix} \tilde{\mathbf{U}}_S \\ \tilde{\mathbf{I}}_S \end{bmatrix} = \mathbf{A}(l_f) \begin{bmatrix} \tilde{\mathbf{U}}_f \\ \tilde{\mathbf{I}}_{f1} \end{bmatrix} \quad (43)$$

The right section can be generally represented as,

$$\begin{bmatrix} \tilde{\mathbf{U}}_R \\ \tilde{\mathbf{I}}_R \end{bmatrix} = \mathbf{A}(l - l_f) \begin{bmatrix} \tilde{\mathbf{U}}_f \\ \tilde{\mathbf{I}}_{f2} \end{bmatrix} \quad (44)$$

With (42) – (44), the line model with fault has the following format [28],

$$\mathbf{z} = f(\mathbf{x}) \quad (45)$$

where,

$$\mathbf{z} = \begin{bmatrix} \tilde{\mathbf{U}}_S \\ \tilde{\mathbf{I}}_S \\ \tilde{\mathbf{U}}_R \\ \tilde{\mathbf{I}}_R \\ \mathbf{0}_{3 \times 1} \end{bmatrix}^T, \quad \mathbf{x} = \begin{bmatrix} \tilde{\mathbf{U}}_f \\ \tilde{\mathbf{I}}_{f1} \\ \tilde{\mathbf{I}}_{f2} \\ l_f \end{bmatrix}^T, \quad \text{and} \quad f(\mathbf{x}) = \begin{bmatrix} \mathbf{A}(l_f) \begin{bmatrix} \mathbf{0}_{3 \times 0} & \mathbf{I}_{3 \times 3} & \mathbf{0}_{3 \times 7} \\ \mathbf{0}_{3 \times 3} & \mathbf{I}_{3 \times 3} & \mathbf{0}_{3 \times 4} \end{bmatrix} \\ \mathbf{A}(l - l_f) \begin{bmatrix} \mathbf{0}_{3 \times 0} & \mathbf{I}_{3 \times 3} & \mathbf{0}_{3 \times 7} \\ \mathbf{0}_{3 \times 6} & \mathbf{I}_{3 \times 3} & \mathbf{0}_{3 \times 1} \end{bmatrix} \\ [-\mathbf{M}_{fault} & \mathbf{I}_{3 \times 3} & \mathbf{I}_{3 \times 3} & \mathbf{0}_{3 \times 1}] \end{bmatrix} \mathbf{x}.$$

There are extensive ways to solve (45). If the line model is rather simplified (eg. phasor domain RL model, etc.), equation (45) can be solved analytically without iterations. For example, for the well-known

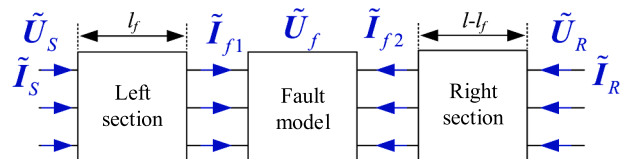


Fig. 20. Line model with fault.

dual-terminal phasor domain method, the line is modelled as the phasor domain scalar form RL model with constant parameters (with the model in 2.9.3). The location is obtained as the following equation [6],

$$l_f = \frac{\tilde{V}_S - \tilde{V}_R + Z_{1L}\tilde{I}_R}{Z_{1L}(\tilde{I}_S + \tilde{I}_R)} \quad (46)$$

where \tilde{V} and \tilde{I} (with subscripts S and R) are calculated according to the phase voltage and current measurements at terminal S and R respectively, as shown in Table 1. Z_{1L} and Z_{0L} are the positive (negative) and zero sequence impedance of the per unit length line, $k_0 = (Z_{0L} - Z_{1L})/Z_{1L}$ is the zero-sequence compensation factor.

However, if the line model becomes rather complex, a general way of solving (45) is introduced. The state estimation algorithm is utilized to solve the fault location. The best estimation of the state vector can be obtained by solving the following optimization problem [28],

$$\min J = (f(\mathbf{x}) - \mathbf{z})^T \mathbf{W}(f(\mathbf{x}) - \mathbf{z}) \quad (47)$$

where $\mathbf{W} = \text{diag}\{\dots, 1/\sigma_i^2, \dots\}$, and σ_i are the error standard deviation of the i -th measurement.

The solution of the best estimated state vector $\hat{\mathbf{x}}$ is given with the following Newton's iteration until convergence,

$$\mathbf{x}^{p+1} = \mathbf{x}^p - (\mathbf{H}^T \mathbf{W} \mathbf{H})^{-1} \mathbf{H}^T \mathbf{W}(f(\mathbf{x}^p) - \mathbf{z}) \quad (48)$$

where $\mathbf{H} = \partial f(\mathbf{x})/\partial \mathbf{x}|_{\mathbf{x}=\mathbf{x}^p}$ is the Jacobean matrix. The fault location is the last element in the state vector $\hat{\mathbf{x}}$.

3.2. Time domain methods

Time domain methods are based on time domain models from section 2.1 to 2.5. Unlike phasor domain methods which require AC sinusoidal steady state assumptions, time domain methods are directly based on sampled-value instantaneous measurements and can be applied to both AC and DC systems, even if the waveforms are experiencing severe transients. Nevertheless, unlike phasor domain methods which typically solve algebraic equations, time domain methods usually need to solve partial or ordinary differential equations, and the way of solving them are more complicated and challenging.

3.2.1. Single-ended time domain methods

Single-ended time domain methods need to build the faulted line model, which consists of two healthy line model and the fault model, as shown in Fig. 21. Here the transmission line model can adopt any time domain healthy transmission line model as shown in Section 2.1-2.5 (e.g. literature [51] adopts the time domain RL model as shown in Section 2.5.4). Afterwards, the solution of the equations can be achieved analytically or numerically.

Take the single-ended time domain fault location method for single phase to ground fault as an example [51]. The diagram of the entire three phase faulted line model is shown in Fig. 21. Here the fault model takes the single phase to ground fault as an example (for different fault type, the fault model is different). The two healthy line models both

Table 1
Values of \tilde{V} and \tilde{I} during different fault types.

Fault type	\tilde{V}	\tilde{I}
A-G	\tilde{V}_A	$\tilde{I}_A + k_0 \tilde{I}_0$
B-G	\tilde{V}_B	$\tilde{I}_B + k_0 \tilde{I}_0$
C-G	\tilde{V}_C	$\tilde{I}_C + k_0 \tilde{I}_0$
A-B, AB-G	$\tilde{V}_A - \tilde{V}_B$	$\tilde{I}_A - \tilde{I}_B$
B-C, BC-G	$\tilde{V}_B - \tilde{V}_C$	$\tilde{I}_B - \tilde{I}_C$
C-A, CA-G	$\tilde{V}_C - \tilde{V}_A$	$\tilde{I}_C - \tilde{I}_A$
ABC, ABC-G	\tilde{V}_A	\tilde{I}_A

adopt the model as shown in Section 2.5.4 as examples. m and n are two ends of the line, l is the length of the entire transmission line, p is the distance between the fault location and end m . The available measurements are the three phase voltages and currents at end m . The unknowns in the entire faulted line model include fault location p , fault resistance R_F , remote-end source equivalent inductance L_R and equivalent resistance R_R .

The equation for the healthy line model is shown in (22) in Section 2.5.4. The equation for the fault model is,

$$u_{Fa}(t) = R_F i_{Fa}(t) \quad (49)$$

where u_{Fa} is the phase A voltage of the transmission line at fault location; i_{Fa} is the phase A fault current flowing into the ground.

The model of the remote-end zero-sequence (zero-mode) equivalent source is also listed [51],

$$0 = u_{n0}(t) + R_{R0} i_{n0}(t) + L_{R0} \cdot di_{n0}(t)/dt \quad (50)$$

where u_{n0} is the zero sequence voltage at end n , i_{n0} is zero sequence current at end n flowing into the line.

Afterwards, the equations (22), (49) and (50) are combined into one single non-linear equation,

$$A_1 p + A_2 R_F + A_3 R_{R0} + A_4 L_{R0} + A_5 R_{R0} p + A_6 L_{R0} p + A_7 R_{R0} R_F + A_8 L_{R0} R_F + A_9 p^2 = B \quad (51)$$

where p , R_F , L_{R0} and R_{R0} are the unknowns to be solved, A_1 - A_9 and B are coefficients only dependent on the voltages and currents at end m , which are known values.

In equation (51), A_1 - A_9 and B are function of time t , and therefore this equation is actually at one time instant t . With the time domain measurements of voltages and currents at end m , a group of equation at different time can be listed. Then the unknowns of p , R_F , L_{R0} and R_{R0} can be solved via the solution of optimization problem using Gauss-Newton algorithm.

In addition, for other fault types (phase to phase, two phase two ground, three phase faults), similar equation of (51) can also be derived. The coefficients of A_1 - A_9 and B are also different, as defined in [51] using the fault component of the voltages and currents at end m .

There are also other single-ended time domain fault location methods. One popular method is the natural frequency based method. The fault location is related to the frequency spectrum of measurements at the local terminal. For example, the dominant frequency can be extracted from the frequency spectrum, and the value of the dominant frequency can be utilized for fault location [52-54]. However, the traditional dominant frequency based methods could experience the challenge of mode mixing phenomenon: during single phase to ground faults, the component of the zero mode can also contribute to the line mode voltages and currents, and the expression of fault location will result in errors. In addition, for the traditional dominant frequency based methods, the identification of the dominant frequency could still be challenging. To overcome above challenges, the entire frequency spectrum can be adopted for natural frequency based fault location [55]. This method systematically solves the mode-mixing phenomenon by accurately model the contribution of different modes to the frequency spectrum. Also, the utilization of entire frequency spectrum avoids extraction of dominant frequency. It is worth noting that the natural frequency based methods usually adopt the time domain lossless distributed parameter line model or the Bergeron model in section 2.5.1.

3.2.2. Dual-ended time domain methods

Dual-ended time domain methods mainly include the **equation solving methods** and the **voltage methods**. The dual-ended **equation solving methods** present the equations of faulted line model, where the fault location is introduced as an unknown variable, and the known

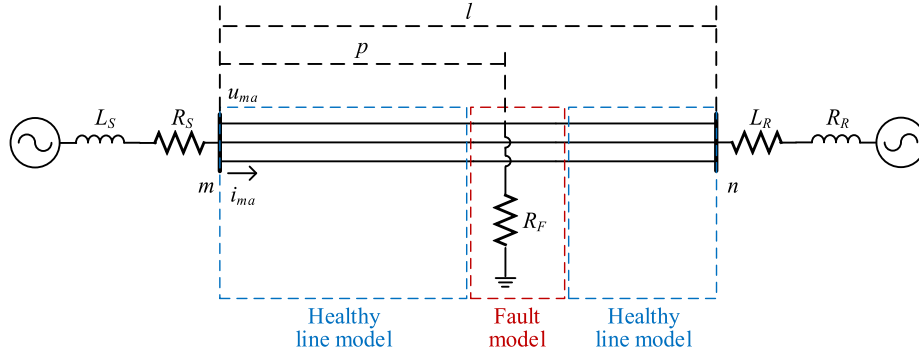


Fig. 21. Diagram of faulted line model.

variables include the dual-ended measurements. Then the fault location is solved via solution of the equations. The **voltage methods** present the healthy line model for the entire transmission line, to solve the voltage distribution from only one end of the line. Then the intersection of the two solved voltage distribution curves from the two ends of the line respectively indicates the fault location.

- (1) Equation solving methods.
- RL equation solving method.

Consider the faulted transmission line mode domain RL model as shown in Fig. 22,

In the figure, the faulted transmission line model of a specific mode (eg. mode 1) is built, with the mode-1 sending end voltage \$u_{S,1}(t)\$ and current \$i_{S,1}(t)\$, receiving end voltage \$u_{R,1}(t)\$ and current \$i_{R,1}(t)\$, fault voltage \$u_{F,1}(t)\$ as well as mode-1 line resistance \$R_1\$ and inductance \$L_1\$ per unit length. The fault voltage can be described with the sending end voltage and current or the receiving end voltage and current, as follows [34],

$$\begin{aligned} u_{F,1}(t) &= u_{S,1}(t) - R_1 l_f i_{S,1}(t) - L_1 l_f di_{S,1}(t)/dt \\ &= u_{R,1}(t) - R_1 (l - l_f) i_{R,1}(t) - L_1 (l - l_f) di_{R,1}(t)/dt \end{aligned} \quad (52)$$

Define the fault location in per centage as \$\lambda = l_f/l\$, equation (52) can be solved with \$\lambda\$ as the unknown [34], where the derivatives can be approximated numerically,

$$\lambda(t) = \frac{u_{S,1}(t) - u_{R,1}(t) + R_1 l i_{R,1}(t) + L_1 l di_{R,1}(t)/dt}{R_1 l i_{S,1}(t) + L_1 l di_{S,1}(t)/dt + R_1 l i_{R,1}(t) + L_1 l di_{R,1}(t)/dt} \quad (53)$$

In equation (53), the solution is a time series. The final fault location \$\eta\$ between 0 and 1 can be determined by solving the following problem [34],

$$\min \sum_{k=1}^n [\lambda(k) - \eta]^2 \quad (54)$$

where \$\lambda(k)\$ is the discrete solution using (53). Note that there are also other ways to solve (52) considering different time instants, such as directly applying the least square methods.

Dynamic state estimation (DSE) based fault location approach.

In the previous section, the time domain RL line model is a simplified but rather inaccurate model. Therefore, the fault location expression is

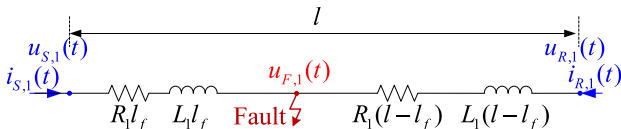


Fig. 22. Faulted transmission time domain RL model.

straightforward but with relatively large fault location error. When the model becomes more accurate and complex, there should be a more systematic way to solve the fault location. Next, the DSE based fault location framework is presented.

In general, the transmission line with fault can be divided into three parts: the left section (healthy line model), the right section (healthy line model) and fault model, as shown in Fig. 23.

Here the three phase line with fault is taken as an example. The time domain matrix form multi-section \$\pi\$ model can be utilized (corresponding to the model in 2.3.1). Other line models such as the models in 2.3 and 2.5 can also be similarly adopted. Note that the models in 2.2 and 2.4 are expressed in PDEs and are not analytical; therefore, the solutions of fault location using the DSE based framework are challenging. In those cases, the voltage method can be utilized, as shown in section 3.2.2 (2).

The left section and right section utilize multi-section \$\pi\$ models with the section numbers \$m\$ and \$n\$, respectively [35]. The model can be built by observing: (a) the voltages at the fault location are the same for the left and the right section; and (b) the two sections are connected by the fault model. The model can be written in the following standard syntax [35–36],

$$\begin{aligned} \mathbf{z}(t) &= \mathbf{Y}_{eqx1} \mathbf{x}(t) + \mathbf{D}_{eqx1} d\mathbf{x}(t)/dt \\ \mathbf{0} &= \mathbf{Y}_{eqx2} \mathbf{x}(t) + \mathbf{D}_{eqx2} d\mathbf{x}(t)/dt \end{aligned} \quad (55)$$

where the state vector is \$\mathbf{x}(t) = [v_1^{(l)}(t), v_2^{(l)}(t), \dots, v_{m+1}^{(l)}(t), v_1^{(r)}(t), \dots, v_{n+1}^{(r)}(t), i_{L1}^{(l)}(t), \dots, i_{Lm}^{(l)}(t), i_{L1}^{(r)}(t), \dots, i_{Ln}^{(r)}(t)]^T\$. \$i_{Lk}^{(a)}\$ is the section current; \$v_k^{(a)}\$ and \$v_{k+1}^{(a)}\$ are the section voltages; \$k\$ means section index (left side of fault: \$k = 1, \dots, m\$ and right side of fault: \$k = 1, \dots, n\$). \$a = l\$ represents sections of left part and \$a = r\$ represents sections of right part. The actual measurement vector is \$\mathbf{z}(t) = [u_s(t), u_r(t), i_s(t), i_r(t)]^T\$,

$$\begin{aligned} \mathbf{Y}_{eqx1} &= \begin{bmatrix} \mathbf{I}_3 & \mathbf{0}_{3 \times (3m+3n)} & \mathbf{0}_{3 \times (3m)} & \mathbf{0}_{3 \times (3n)} \\ \mathbf{0}_{3 \times (3m+3n)} & \mathbf{I}_3 & \mathbf{0}_{3 \times (3m)} & \mathbf{0}_{3 \times (3n)} \\ \mathbf{G}_l/2 & \mathbf{0}_{3 \times (3m+3n)} & \mathbf{I}_3 & \mathbf{0}_{3 \times (3m+3n-3)} \\ \mathbf{0}_{3 \times (3m+3n)} & \mathbf{G}_r/2 & \mathbf{0}_{3 \times (3m+3n-3)} & -\mathbf{I}_3 \end{bmatrix} \mathbf{Y}_{eqx2} \\ &= \begin{bmatrix} \mathbf{Y}_{11} & \mathbf{0}_{(3m-3) \times (3n+3)} & \mathbf{E}_{3m-3} & \mathbf{0}_{(3m-3) \times (3n)} \\ \mathbf{0}_{(3n-3) \times (3m+3)} & \mathbf{Y}_{22} & \mathbf{0}_{(3n-3) \times (3m+3)} & \mathbf{E}_{3n-3} \\ \mathbf{E}_{3m} & \mathbf{0}_{(3m) \times (3n)} & \mathbf{Y}_{33} & \mathbf{0}_{(3m) \times (3n)} \\ \mathbf{0}_{(3n) \times (3m)} & \mathbf{E}_{3n} & \mathbf{0}_{(3n) \times (3m)} & \mathbf{Y}_{44} \\ \mathbf{Y}_{51} & \mathbf{0}_{3 \times (3m+3n-3)} & \mathbf{Y}_{53} & \mathbf{0}_{3 \times (3n-3)} \end{bmatrix} \mathbf{D}_{eqx1} \\ &= \begin{bmatrix} \mathbf{0}_{3 \times (3m+3)} & \mathbf{0}_{3 \times (3n)} & \mathbf{0}_{3 \times (3m)} & \mathbf{0}_{3 \times (3n)} \\ \mathbf{0}_{3 \times (3m+3)} & \mathbf{0}_{3 \times (3n)} & \mathbf{0}_{3 \times (3m)} & \mathbf{0}_{3 \times (3n)} \\ \mathbf{C}_l/2 & \mathbf{0}_{3 \times (3m+3n)} & \mathbf{0}_{3 \times (3m)} & \mathbf{0}_{3 \times (3n)} \\ \mathbf{0}_{3 \times (3m+3n)} & \mathbf{C}_r/2 & \mathbf{0}_{3 \times (3m)} & \mathbf{0}_{3 \times (3n)} \end{bmatrix} \mathbf{D}_{eqx2} \\ &= \begin{bmatrix} \mathbf{D}_{11} & \mathbf{0}_{(3m-3) \times (3n+3)} & \mathbf{0}_{(3m-3) \times (3m)} & \mathbf{0}_{(3m-3) \times (3n)} \\ \mathbf{0}_{(3n-3) \times (3m+3)} & \mathbf{D}_{22} & \mathbf{0}_{(3n-3) \times (3m+3)} & \mathbf{0}_{(3n-3) \times (3n)} \\ \mathbf{0}_{(3m) \times (3m+3)} & \mathbf{0}_{(3m) \times (3n)} & \mathbf{D}_{33} & \mathbf{0}_{(3m) \times (3n)} \\ \mathbf{0}_{(3n) \times (3m)} & \mathbf{0}_{(3n) \times (3n+3)} & \mathbf{0}_{(3n) \times (3m)} & \mathbf{D}_{44} \\ \mathbf{D}_{51} & \mathbf{0}_{3 \times (3m+3n-3)} & \mathbf{0}_{3 \times 6} & \mathbf{0}_{3 \times (3n-3)} \end{bmatrix} \end{aligned}$$

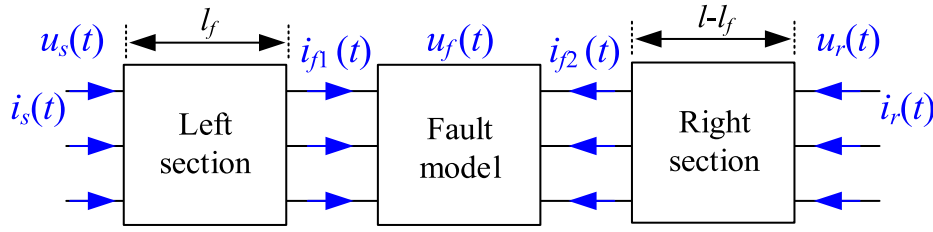


Fig. 23. Line model with fault in time domain.

\mathbf{I}_j is the identity matrix with the dimension of j , $\mathbf{0}_{j \times k}$ is the zero matrix with the dimension of $j \times k$, $\mathbf{Y}_{11} = [\mathbf{0}_{(3m-3) \times 3} \quad \mathbf{G}]$. \mathbf{G} is a block diagonal matrix with $m-1$ \mathbf{G}_l matrices along the diagonal. $\mathbf{Y}_{51} = [\mathbf{0}_{3 \times (3m)} \quad \mathbf{M}_{fault} - (\mathbf{G}_l + \mathbf{G}_r)/2]$, $\mathbf{Y}_{53} = [-\mathbf{I}_3 \quad \mathbf{I}_3]$. \mathbf{Y}_{22} , \mathbf{Y}_{33} , \mathbf{Y}_{44} are block diagonal matrices with $n-1$ \mathbf{G}_r matrices, m \mathbf{R}_l matrices and n \mathbf{R}_r matrices along the diagonal, respectively. $\mathbf{E}_j = [\mathbf{0}_{j \times 3} \quad \mathbf{I}_j] - [\mathbf{I}_j \quad \mathbf{0}_{j \times 3}]$. $\mathbf{D}_{11} = [\mathbf{0}_{(3m-3) \times 3} \quad \mathbf{C}]$, \mathbf{C} is a block diagonal matrix with $m-1$ \mathbf{C}_l matrices along the diagonal. $\mathbf{D}_{51} = [\mathbf{0}_{3 \times (3m)} \quad -(\mathbf{C}_l + \mathbf{C}_r)/2]$; \mathbf{D}_{22} , \mathbf{D}_{33} , \mathbf{D}_{44} are block diagonal matrices with $n-1$ \mathbf{C}_r matrices, m \mathbf{L}_l matrices and n \mathbf{L}_r matrices along the diagonal, respectively. $\mathbf{R}_l = \mathbf{R}_l \cdot l_f/m$, $\mathbf{L}_l = \mathbf{L}_l \cdot l_f/m$, $\mathbf{G}_l = \mathbf{G}_l \cdot l_f/m$, $\mathbf{C}_l = \mathbf{C}_l \cdot l_f/m$, $\mathbf{R}_r = \mathbf{R}_r \cdot (l-l_f)/n$, $\mathbf{L}_r = \mathbf{L}_r \cdot (l-l_f)/n$, $\mathbf{G}_r = \mathbf{G}_r \cdot (l-l_f)/n$, $\mathbf{C}_r = \mathbf{C}_r \cdot (l-l_f)/n$, \mathbf{R}_l , \mathbf{L}_l , \mathbf{G}_l and \mathbf{C}_l are series resistance, series reactance, shunt conductance and shunt capacitance matrices per unit length, with the dimension of 3 by 3, \mathbf{M}_{fault} is provided in the fault model, R_f is the fault resistance, and l_f is the fault location.

It can be clearly observed from (55) that, although the format of the line model with fault is linear, the fault location problem itself is highly nonlinear, as the unknown variable l_f is within the coefficient matrices and is strongly coupled with the state vector $\mathbf{x}(t)$ of the system.

The DSE algorithms are widely adopted in tracking transients of power systems and to solve unknown variables [2,56–57]. Specifically, to solve the unknown l_f for the highly nonlinear problem in (55), the DSE algorithm can be utilized [35]. One way is to directly solve the nonlinear problem in (55), by introducing unknown parameters such as the fault location and the fault resistance as augmented states of the system. In those cases, the DSE methods can be applied to solve the states of the system including the fault location [35]. However, due to the limited length of the available time window during the fault and high nonlinearity of the problem, the states may not converge within this small period of time.

Therefore, the following method combining DSE and optimization methods (such as gradient descent) is presented to improve the fault location performances [36]. The key idea is to convert the nonlinear DSE problem into several linear DSE problems, and use optimization tools to find fault location. First, with a given pair of fault location and fault resistance, the fault location problem in (55) becomes linear, and DSE solving linear problem is much faster with much improved convergence characteristics. To eliminate the differential terms in (55), the numerical integration methods such as the quadratic integration can be utilized. The algebraic form of the linear dynamic line model is,

$$\mathbf{z}(t, t_m) = \mathbf{Y}_{eqx} \mathbf{x}(t, t_m) - \mathbf{B}_{eq} \quad (56)$$

where $t_m = t - \Delta t$, Δt is the sampling interval of the system, $\mathbf{x}(t, t_m) = [\mathbf{x}(t), \mathbf{x}(t_m)]^T$, $\mathbf{z}(t, t_m) = [\mathbf{z}(t), \mathbf{0}, \mathbf{z}(t_m), \mathbf{0}]^T$, $\mathbf{B}_{eq} = -\mathbf{N}_{eqx} \cdot \mathbf{x}(t - 2\Delta t) - \mathbf{M}_{eq} \cdot \mathbf{z}(t - 2\Delta t)$, and,

$$\mathbf{Y}_{eqx} = \begin{bmatrix} \mathbf{Y}_{eqx1} + 2\mathbf{D}_{eqx1}/\Delta t & -4\mathbf{D}_{eqx1}/\Delta t \\ \mathbf{Y}_{eqx2} + 2\mathbf{D}_{eqx2}/\Delta t & -4\mathbf{D}_{eqx2}/\Delta t \\ \mathbf{D}_{eqx1}/(4\Delta t) & \mathbf{Y}_{eqx1} + \mathbf{D}_{eqx1}/\Delta t \\ \mathbf{D}_{eqx2}/(4\Delta t) & \mathbf{Y}_{eqx2} + \mathbf{D}_{eqx2}/\Delta t \end{bmatrix}, \mathbf{N}_{eqx} = \begin{bmatrix} -\mathbf{Y}_{eqx1} + 2\mathbf{D}_{eqx1}/\Delta t \\ -\mathbf{Y}_{eqx2} + 2\mathbf{D}_{eqx2}/\Delta t \\ \mathbf{Y}_{eqx1}/2 - 5\mathbf{D}_{eqx1}/(4\Delta t) \\ \mathbf{Y}_{eqx2}/2 - 5\mathbf{D}_{eqx2}/(4\Delta t) \end{bmatrix}, \mathbf{M}_{eq} = \begin{bmatrix} \mathbf{I}_3 \\ \mathbf{0}_{(6m+6n-3) \times 3} \\ -0.5\mathbf{I}_3 \\ \mathbf{0}_{(6m+6n-3) \times 3} \end{bmatrix}.$$

The problem can be formulated as the following optimization problem. As mentioned before, the fault location l_f and R_f are given,

$$\min_{\mathbf{x}(t, t_m)} J(t) = \mathbf{r}(t, t_m)^T \mathbf{W} \mathbf{r}(t, t_m) \quad (57)$$

where the residual is defined as the difference between the estimated measurements and actual measurements $\mathbf{r}(t, t_m) = \mathbf{Y}_{eqx} \mathbf{x}(t, t_m) - \mathbf{B}_{eq} - \mathbf{z}(t, t_m)$, where the weight matrix is $\mathbf{W} = \text{diag}\{1/\sigma_1^2, 1/\sigma_2^2, \dots\}$, and σ_i is the i^{th} measurement standard deviation in $\mathbf{z}(t, t_m)$.

Since the model is linear, the solution at each time step can be obtained without iteration, as follows,

$$\hat{\mathbf{x}}(t, t_m) = (\mathbf{Y}_{eqx}^T \mathbf{W} \mathbf{Y}_{eqx})^{-1} \mathbf{Y}_{eqx}^T \mathbf{W} (\mathbf{z}(t, t_m) + \mathbf{B}_{eq}) \quad (58)$$

Finally, substitute the solution $\mathbf{x}(t, t_m) = \hat{\mathbf{x}}(t, t_m)$ into (57) to obtain the $\hat{J}(t)$. It can be clearly observed that the value of $\hat{J}(t)$ is a function of l_f and R_f . The value of $\hat{J}(t)$ quantifies the consistency between the measurements and the dynamic line model. If the consistency is low (i.e. $\hat{J}(t)$ is high), the line model is incorrect and it is because the given l_f and R_f are far from the true value; if the consistency is high (i.e. $\hat{J}(t)$ is small), the given l_f and R_f are close to the true value. To also take time t into account, the average value (y) of $\hat{J}(t)$ within a user-defined time window can be selected to quantify the consistency. The fault location can be achieved when the value of y reaches the minimum [36],

$$\min_{l_f, R_f} y = \chi(l_f, R_f) \quad (59)$$

where $\chi(\cdot)$ expresses y as function of l_f and R_f .

To solve the optimization problem, here the gradient descent method is adopted as an example [36]. The iterative procedure is,

$$[l_f^{(v)}, R_f^{(v)}] = [l_f^{(v-1)}, R_f^{(v-1)}] - \alpha^{(v)} \nabla \chi(l_f^{(v-1)}, R_f^{(v-1)}) \quad (60)$$

where $\alpha^{(v)}$ is the step size and $\nabla \chi(l_f^{(v-1)}, R_f^{(v-1)})$ is the gradient that could be numerically calculated through (61), where Δl_f and ΔR_f are small perturbations

$$\nabla \chi(l_f^{(v)}, R_f^{(v)}) = \begin{bmatrix} (\chi(l_f^{(v)} + \Delta l_f, R_f^{(v)}) - \chi(l_f^{(v)}, R_f^{(v)}))/\Delta l_f \\ (\chi(l_f^{(v)}, R_f^{(v)} + \Delta R_f) - \chi(l_f^{(v)}, R_f^{(v)}))/\Delta R_f \end{bmatrix}^T \quad (61)$$

(2) Voltage method.

Another more general way of solving the fault location in time domain is to use the voltage method [38–44]. The main idea is as follows. After the fault occurs, one can first assume the healthy transmission line model, and solve the voltage distribution along entire transmission line from single end of the line. Then the voltage distribution is only correctly solved before the fault location. For example, the voltage distribution $u(x, t)$ solved from the left terminal is correct only when x is within the range $[0, l_f]$, where l_f is the fault location from the left terminal. For the voltage distribution calculated from another end, the $u(x, t)$ is only correct when x is within the range of $[l_f, l]$, where l is the line length. Therefore, for the two voltage distribution curves calculated from two ends respectively, only the voltage at fault location $u(l_f)$ is calculated identically. The intersection of the two voltage

distribution curves shows the fault location. The voltage methods usually take following equation to determine the fault location [43].

$$\min_f(x, t) = \min_x \sum_{t=t_1}^{t_2} |u^{(k)}(x, t) - u^{(m)}(x, t)| \quad (62)$$

where $u^{(k)}(x, t)$ and $u^{(m)}(x, t)$ are the voltage distribution calculated from line terminals k and m , respectively. $[t_1, t_2]$ is the summation window.

In equation (62), the voltage distributions of $u^{(k)}(x, t)$ and $u^{(m)}(x, t)$ can be solved using any time domain healthy transmission line model as shown in Section 2.1-2.5, from very simplified scalar form RL model to complicated matrix form PDE line model. Note that the framework of the voltage method fault location does not require models with analytical expressions. Taking the following voltage methods as examples. Literature [43] adopts the model in Section 2.2; literature [42] adopts the model in Section 2.4; literatures [38–41] adopt the model in Section 2.5.1. For most of those approaches, the voltage distribution is discretely calculated at different distance (e.g. $u(k\Delta x, t)$, $k = 0, 1, \dots, N_x$ is solved, where Δx is the distance interval, and $N_x\Delta x$ is the length of entire transmission line). Therefore, to reduce the computation complexity, a two-iteration algorithm can usually be adopted in many voltage methods as shown in Fig. 24 [42–43], where k and m are two ends of the line. The first iteration calculates the approximate fault location x_{iter1} with a relatively large distance interval Δx_{iter1} , within the length of the entire line $[0, l]$. The second iteration fine-tunes the accurate fault location x_{iter2} with smaller distance interval Δx_{iter2} , within the length of line segment $[x_{iter1} - \Delta x_{iter1}, x_{iter1} + \Delta x_{iter1}]$.

For the solution of the voltage distribution using different transmission line model, the methods are briefly reviewed here. In [43], the solution of voltage distribution is obtained via numerical solution of PDE in (3) with finite difference method. The solution is,

$$\begin{aligned} U_{j+1}^n = & -U_{j-1}^n + (2E - 2\Delta x^2/\Delta t^2 \cdot B_1 + \Delta x^2 B_3)U_j^n + (\Delta x^2/\Delta t^2 \cdot B_1 \\ & - \Delta x^2/2\Delta t \cdot B_2)U_{j-1}^{n-1} + (\Delta x^2/\Delta t^2 \cdot B_1 + \Delta x^2/2\Delta t \cdot B_2)U_j^{n-1} \end{aligned} \quad (63)$$

where the approximate numerical solution is expressed as the capital letter variable with the subscript j as the distance step number and the superscript n as the time step number. Δx and Δt are the distance interval and time interval, respectively. $B_1 = LC$, $B_2 = RC + LG$, $B_3 = RG$. E is the identity matrix with the dimension of M , and M is the phase number. It is worth noting that the stability condition of the numerical format is strictly proved, and the minimum numerical error of the numerical format is strictly derived [43]. The distance and time intervals of the numerical solution should be selected properly to ensure numerical stability and minimum numerical error.

In [42], the solution of voltage distribution is obtained via numerical solution of simplified PDE in (13) with trapezoidal integration. The solution is,

$$\begin{aligned} U_j^n = & 1/2 \cdot [U_{j-1}^{n-1} + U_{j-1}^{n+1}] + Z_c/2 \cdot [I_{j-1}^{n-1} - I_{j-1}^{n+1}] + R\Delta x/4 \cdot [I_{j-1}^{n-1} \\ & + I_{j-1}^{n+1}] - R\Delta x/2 \cdot I_j^n \end{aligned} \quad (64)$$

where the definition of approximate numerical solution is similar as those in (63), and $Z_c = \sqrt{L/C}$.

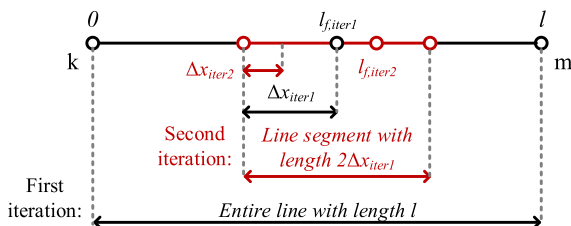


Fig. 24. Two-iteration fault location algorithm.

In [38–41], the solution of voltage distribution is obtained via the Bergeron model (17). From (17), the voltage at one end of the line can be expressed only using the voltage and current at another end of the line as shown in (65). Afterwards, with different settings of the line length (coefficients of Z_j , h and τ are influenced by the line length), the voltage distribution, i.e. the $u_{R,j}(t)$ at different location, can be solved.

$$\begin{aligned} u_{R,j}(t) = & 2Z_j/(1+h)^2 \cdot [1/Z_j \cdot u_{S,j}(t+\tau) - i_{S,j}(t+\tau)] - [(1-h_j)/(1+h_j)]^2 \cdot u_{S,j}(t) \\ & - 2h(1-h)/(1+h)^2 \cdot Z_j i_{S,j}(t) + 2h^2/(1+h)^2 \cdot Z_j [1/Z_j \cdot u_{S,j}(t-\tau) + h \cdot i_{S,j}(t-\tau)] \end{aligned} \quad (65)$$

where the definitions of Z_j , h and τ are same as those in (17).

3.3. Summary

Line model can well describe the physical laws that the line of interest obeys. The proper selection of a line model is a prerequisite for designing accurate model-based line protection functions and fault location algorithms. To sum up, the phasor domain methods are compatible with practical fault location problems in exclusively AC transmission grids. In addition, the available time window of measurements during faults should be long enough (eg. typically longer than 1 fundamental cycle) to extract accurate phasor measurements. Time domain methods are compatible with practical fault location problems in both AC and DC transmission lines, even with extreme short time window of measurements after the occurrence of the fault.

Time domain approaches also have their own features. First, compared to phasor domain approaches that are typically based on algebraic equations, time domain fault location methods usually need to solve differential equations and are more complicated. Second, time domain methods are more sensitive to frequency dependent line parameters, since they utilize waveforms with a wide frequency range. In comparison, phasor domain methods does not suffer from frequency dependency of line parameters, since the phasors correspond exactly to the fundamental frequency: in this case, using parameters at the fundamental frequency for phasor domain fault location will avoid the issue of frequency dependent parameters. It is worth noting that phasor domain methods usually analyze the steady state during the fault. During the steady state, the frequency dependent line parameters would also have less influence on the time domain methods.

Spectral domain fault location algorithms, e.g. [74], rely on voltage and current phasors, traditionally obtained using e.g. Discrete Fourier Transform (DFT). Filtering out phasors requires time, what is related to the size of the applied data window, e.g. 20–40 ms. This is slowing down the algorithm and prolonging the algorithm convergence. On the other hand, time-domain algorithms, e.g. [63–65], have significantly faster convergence properties and are not sensitive to decaying DC component existing in fault current. The algorithm speed is more critical in real-time applications, e.g. when designing distance protection, whereas when it comes to fault location, from the practical viewpoint, it is not essential.

4. Validations via numerical experiments

In this section, various model-based fault location methods are studied and compared in an example test system. The example test system is built in PSCAD/EMTDC. The line of interest is a 500 kV 200 km HVAC two-terminal untransposed transmission line. The nominal frequency of the system is 50 Hz. Meanwhile, the frequency dependent model (phase) of the transmission line in PSCAD/EMTDC is adopted to ensure the practicability during numerical experiments. The equivalent source impedances are $10\angle 80^\circ \Omega$ and $15\angle 75^\circ \Omega$ at the sending and the receiving end, respectively. The phase angles of the equivalent sources at the sending and the receiving end are 30° and 0° , respectively. Three phase sampled-value instantaneous voltage and current measurements are installed at both terminals of the transmission line. The instantaneous voltages and currents are captured using 4000 samples/second

(80 samples/cycle) sampling rate according to IEC61850-9-2 standard [19]. If phasor domain approaches are adopted, the phasors are extracted according to IEEE C37.118 standard [31]. Note that the traveling wave based methods will encounter huge systematic errors (in the order of tens of kilometers) if this low sampling rate of 4000 samples/second is adopted.

The line series impedance and shunt admittance matrices per meter at 50 Hz are shown as follows,

$$Z_{abc} = \begin{bmatrix} 0.0900 + j0.4714 & 0.0880 + j0.2579 & 0.0840 + j0.2179 \\ 0.0880 + j0.2579 & 0.0979 + j0.4669 & 0.0880 + j0.2579 \\ 0.0840 + j0.2179 & 0.0880 + j0.2579 & 0.0900 + j0.4714 \end{bmatrix} \\ \times 10^{-3} \text{ (ohms/m)}$$

$$Y_{abc} = \begin{bmatrix} 0.001 + j0.4195 & -j0.1013 & -j0.0304 \\ -j0.1013 & 0.001 + j0.4562 & -j0.1013 \\ -j0.0304 & -j0.1013 & 0.001 + j0.4195 \end{bmatrix} \\ \times 10^{-8} \text{ (mhos/m)}$$

Next, the performances of various model-based phasor domain and time domain fault location methods are presented and compared as examples, to demonstrate the importance of accurate line modeling and its impact on fault location accuracy. The fault location error is defined as,

$$\text{Fault Location Error} = \frac{|\text{Estimated Fault Location} - \text{Actual Fault Location}|}{\text{Entire Length of the Line}} \\ \times 100\% \quad (66)$$

4.1. Phasor domain methods

For phasor domain approaches, for simplicity, the voltage and current phasors at both terminals are extracted when the system during faults is close to steady-state operation: the average phasor values corresponding to the 3rd to 4th cycle after the occurrence of the fault are utilized. In this case, the phasor domain approach assumes that the available measurements during faults are relatively long; otherwise, phasor extraction inaccuracies will propagate to the fault location results. Of course, even if the time window is relatively short (eg. around 1–2 cycles), there are also phasor extraction methods that can accurately extract phasors during transients [32–33].

Here, three single-end phasor domain approaches in section 3.1.1 and three dual-ended phasor domain approaches in section 3.1.2 are listed as examples:

- (1) traditional single-ended impedance-based fault location methods [6], where the line is modelled as phasor domain scalar form lumped R-L model in section 2.9.3;
- (2) Takagi single-ended impedance-based fault location method [47], with the assumption of homogeneity of source and line impedances;
- (3) Eriksson single-ended impedance-based fault location method [49], with known remote terminal source impedance;
- (4) traditional dual-ended impedance-based fault location method [6], where the line is modelled as phasor domain scalar form lumped R-L model in section 2.9.3, and symmetrical component transformation in (32) is adopted;
- (5) dual-ended scalar form fully distributed parameter model-based fault location method [28], where the line is modelled as phasor domain scalar form fully distributed parameter model in section 2.8, and symmetrical component transformation in (32) is adopted;
- (6) dual-ended matrix form fully distributed parameter model-based fault location method [28], where the line is modelled as phasor

domain matrix form fully distributed parameter model in section 2.6.

Note that for (1) to (5), the symmetrical component transformation is adopted to decouple the three phase line. However, this decoupling assumes symmetrical structures of transmission lines, which will cause fault location errors for transmission lines with asymmetrical tower structures. For (6), the matrix form line model is adopted and asymmetry of the tower structure is fully considered.

In the following figures in part 4, single ended phasor domain methods (1), (2) and (3) are referred as “Simple reactance method”, “Takagi method”, and “Eriksson method”, respectively. Dual ended phasor domain methods (4), (5) and (6) are referred as “RL method”, “Fully distributed parameter model-based method (assuming symmetry)”, and “Fully distributed parameter model-based method (considering asymmetry)”, respectively.

4.1.1. Single ended phasor domain methods

Next, several groups of A-G, B-C, BC-G and three phase faults with 1 Ω fault resistance are studied. In addition, several groups of A-G faults with 10 Ω and 100 Ω fault resistances are studied to consider high resistance faults. The results of 3 single ended phasor domain methods are shown in Fig. 25. The average and maximum fault location errors are provided in Table 3.

It can be observed that the three methods show comparable fault location error during low resistance faults. It can also be observed that the Eriksson method presents higher fault location accuracy than other two methods especially during single phase to ground high resistance faults, since it can well consider the contribution of the remote side fault current to the line voltage at the fault location. However, three methods are with relatively large fault location errors since the line is assumed to be transposed. In addition, the errors are relatively large when the faults are far away from the local terminal, due to the modeling error of the phasor domain lump RL model.

4.1.2. Dual ended phasor domain methods

Next, similarly, several groups of A-G, B-C, BC-G and three phase faults with 1 Ω fault resistance are studied. In addition, several groups of A-G faults with 10 Ω and 100 Ω fault resistances are studied to consider high resistance faults. The results of 3 dual ended phasor domain methods are shown in Fig. 26. The average and maximum fault location errors are provided in Table 4.

One can observe that method (6) demonstrates less errors than methods (4) and (5), since method (6) is based on the fully distributed parameter line model and at the same time fully considers line asymmetry. Method (6) also shows much reduced errors than methods (1) (2) and (3). These results clearly demonstrate the importance to accurately model the transmission line of interest.

4.2. Time domain methods

For time domain approaches, they do not assume steady state operation of the system. Therefore, they are compatible with short data window after the occurrence of the fault, where the line is equipped with fast-tripping techniques. Here for all time domain approaches, the voltage and current measurements within only 10 ms (half a cycle) after the occurrence of the fault are utilized. Note that the phasors during faults cannot be accurately extracted with such a short time window.

Here, four dual-ended time domain approaches in section 3.2.2 are listed as examples:

- (1) dual-ended R-L model-based fault location method [34], where the line is modelled as time domain scalar form lumped R-L model in section 2.5.4, and Clarke transformation in (11) is adopted;

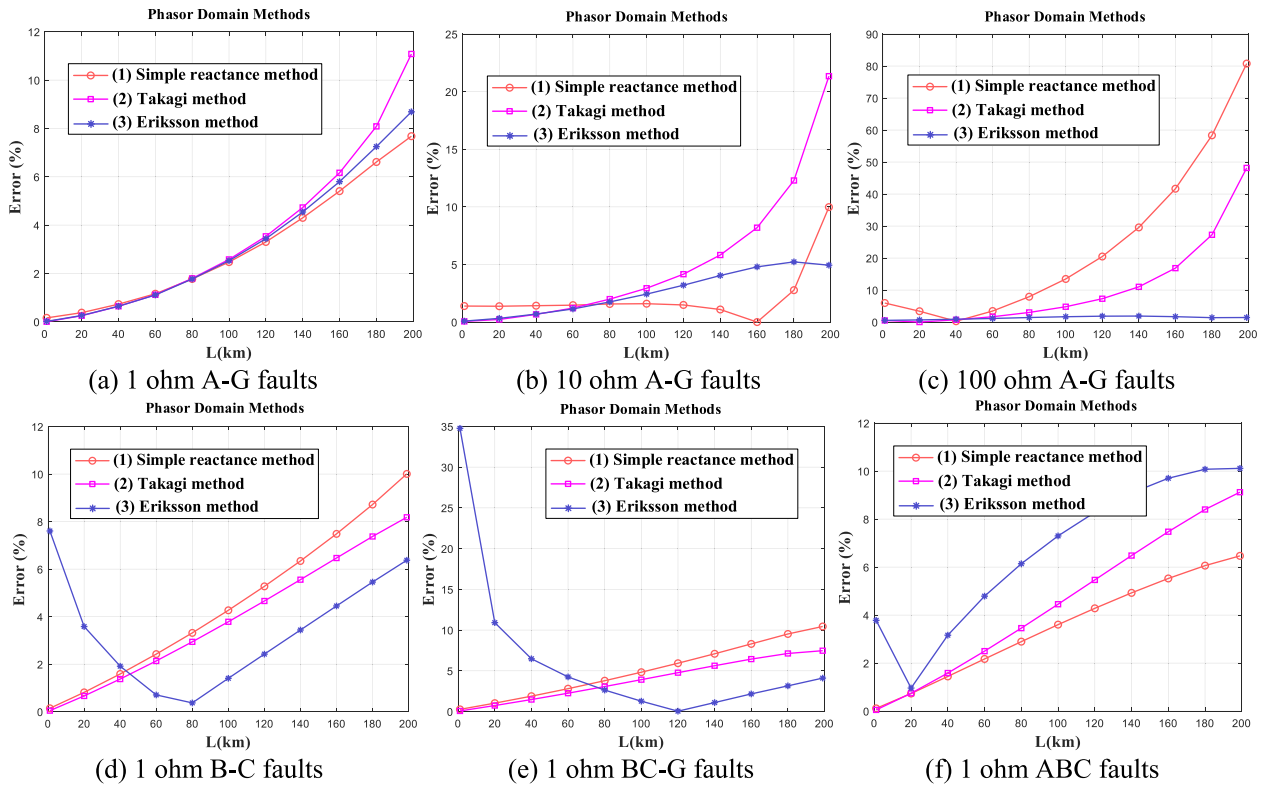


Fig. 25. Fault location results comparison, various single ended phasor domain fault location approaches.

Table 2

Values of M_{fault} during different fault types.

Fault type	M_{fault}	Fault type	M_{fault}	Fault type	M_{fault}	Fault type	M_{fault}
A-G	$Y_f \begin{bmatrix} 1 & 0 & 0 \\ 0 & 0 & 0 \\ 0 & 0 & 0 \end{bmatrix}$	B-G	$Y_f \begin{bmatrix} 0 & 0 & 0 \\ 0 & 1 & 0 \\ 0 & 0 & 0 \end{bmatrix}$	C-G	$Y_f \begin{bmatrix} 0 & 0 & 0 \\ 0 & 0 & 0 \\ 0 & 0 & 1 \end{bmatrix}$	A-B	$Y_f \begin{bmatrix} 1 & -1 & 0 \\ -1 & 1 & 0 \\ 0 & 0 & 0 \end{bmatrix}$
B-C	$Y_f \begin{bmatrix} 0 & 0 & 0 \\ 0 & 1 & -1 \\ 0 & -1 & 1 \end{bmatrix}$	A-C	$Y_f \begin{bmatrix} 1 & 0 & -1 \\ 0 & 0 & 0 \\ -1 & 0 & 1 \end{bmatrix}$	ABG	$Y_f \begin{bmatrix} 1 & 0 & 0 \\ 0 & 1 & 0 \\ 0 & 0 & 0 \end{bmatrix}$	BCG	$Y_f \begin{bmatrix} 0 & 0 & 0 \\ 0 & 1 & 0 \\ 0 & 0 & 1 \end{bmatrix}$
ACG	$Y_f \begin{bmatrix} 1 & 0 & 0 \\ 0 & 0 & 0 \\ 0 & 0 & 1 \end{bmatrix}$	3 phase fault	$Y_f \begin{bmatrix} 1 & 0 & 0 \\ 0 & 1 & 0 \\ 0 & 0 & 1 \end{bmatrix}$				

Table 3

Average and Maximum Errors, Various Single Ended Phasor Domain Fault Location Approaches.

Fault location methods	A-G 1 Ω Faults		A-G 10 Ω Faults		A-G 100 Ω Faults	
	Averageerror (%)	Maxerror (%)	Averageerror (%)	Maxerror (%)	Averageerror (%)	Maxerror (%)
(1) Simple reactance method	3.0889	7.6800	2.1957	9.9789	24.1200	80.7739
(2) Takagi method	3.8166	12.2391	5.3552	21.3453	11.0277	48.1659
(3) Eriksson method	3.2774	8.6888	2.6015	5.2258	1.3229	1.8813
Fault location methods	B-C 1 Ω Faults		BC-G 1 Ω Faults		ABC 1 Ω Faults	
	Averageerror (%)	Maxerror (%)	Averageerror (%)	Maxerror (%)	Averageerror (%)	Maxerror (%)
(1) Simple reactance method	4.5805	10.0064	5.0794	10.4399	3.4757	6.4689
(2) Takagi method	3.9260	8.1815	3.9029	7.4675	4.5219	9.1227
(3) Eriksson method	3.4305	7.6059	6.4426	34.7632	6.6730	10.1148

- (2) dual-ended Bergeron model-based fault location method [38], where the line is modelled as time domain scalar form Bergeron model in section 2.5.1, and Clarke transformation in (11) is adopted;
- (3) dual-ended DSE based fault location method [36], where the line is modelled as time domain matrix form multi-section π model in section 2.3.1;
- (4) dual-ended numerical solutions of PDE (NSPDE) based fault location method [43], where the line is modelled as time domain

matrix form fully distributed parameter line model (PDEs) in section 2.2.

Note that for (1) and (2), the Clarke transformation is adopted to decouple the three phase line. However, similar as the symmetrical component transformation, this decoupling also assumes symmetrical structures of transmission lines, which will cause fault location errors for transmission lines with asymmetrical tower structures. For (3) and (4), the matrix form line models are adopted and asymmetry of the tower

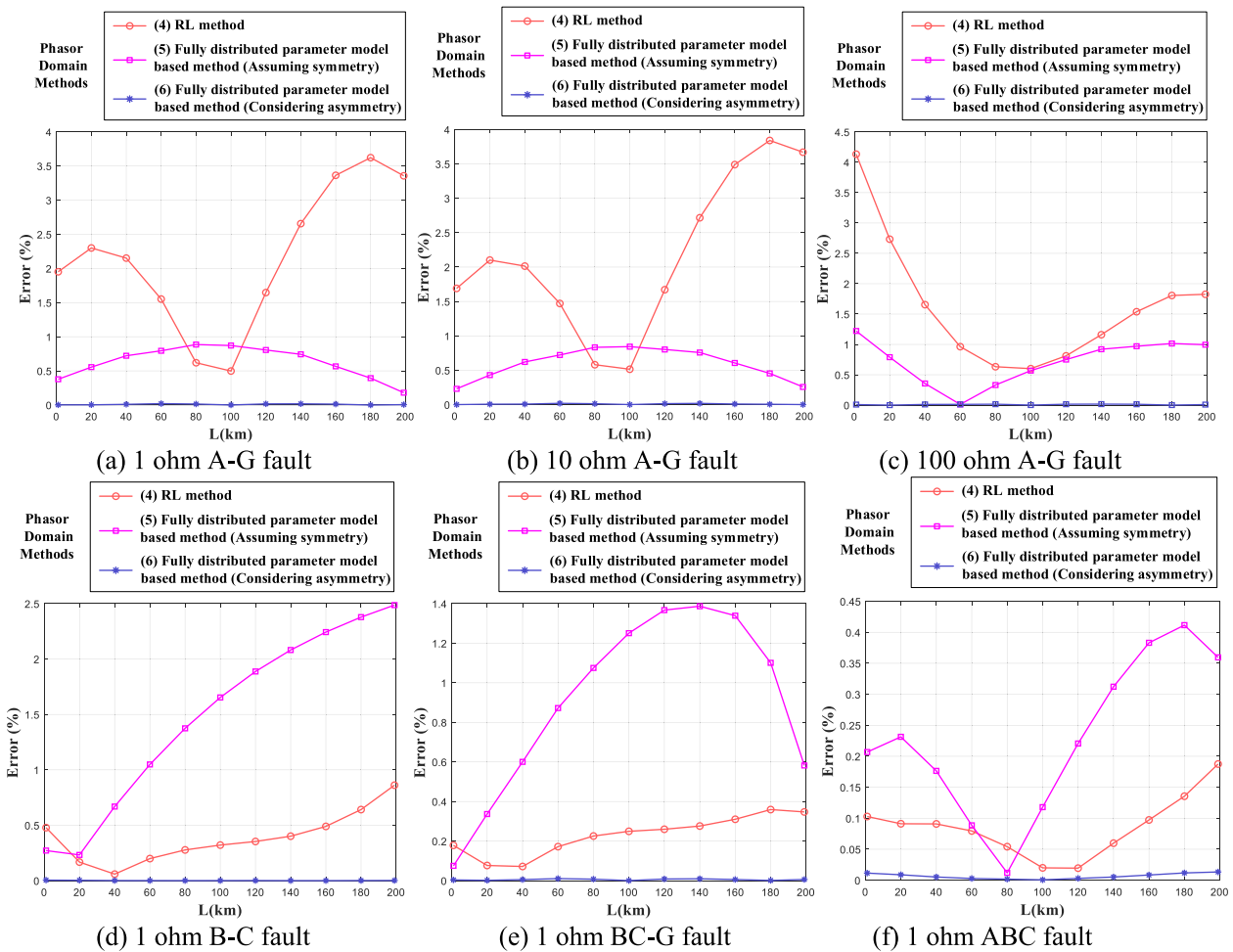


Fig. 26. Fault location results comparison, various dual ended phasor domain fault location approaches.

Table 4
Average and maximum errors, various dual ended phasor domain fault location approaches.

Fault location methods	A-G 1 Ω Faults		A-G 10 Ω Faults		A-G 100 Ω Faults	
	Averageerror (%)	Maxerror (%)	Averageerror (%)	Maxerror (%)	Averageerror (%)	Maxerror (%)
(4) RL method	2.1559	3.6220	2.1598	3.8404	1.6237	4.1339
(5) Fully distributed parameter model-based method (Assuming symmetry)	0.6268	0.8856	0.5959	0.8431	0.7210	1.2217
(6) Fully distributed parameter model-based method (Considering asymmetry)	0.0099	0.0209	0.0088	0.0192	0.0098	0.0170
Fault location methods	B-C 1 Ω Faults		BC-G 1 Ω Faults		ABC 1 Ω Faults	
	Averageerror (%)	Maxerror (%)	Averageerror (%)	Maxerror (%)	Averageerror (%)	Maxerror (%)
(4) RL method	0.3862	0.8616	0.2296	0.3592	0.0853	0.1875
(5) Fully distributed parameter model-based method (Assuming symmetry)	1.4843	2.4871	0.9079	1.3870	0.2291	0.4116
(6) Fully distributed parameter model-based method (Considering asymmetry)	0.0013	0.0049	0.0054	0.0104	0.0066	0.0134

structure is fully considered. In the following figures of section 4, time domain methods (1), (2), (3) and (4) are referred as “RL method”, “Bergeron method”, “DSE method” and “NSPDE method”, respectively.

Next, several groups of A-G, B-C, BC-G and three phase faults with 1 Ω fault resistance are studied. In addition, several groups of A-G faults with 10 Ω and 100 Ω fault resistances are studied to consider high resistance faults. The results of 4 time domain methods are shown in Fig. 27. The average and maximum fault location errors are provided in Table 5. First, generally speaking, method (2) demonstrates smaller fault location errors compared to method (1), since the Bergeron line model in

method (2) presents higher fault location accuracy than the lumped RL line model. However, it can be observed that methods (1) and (2) have larger errors in comparison to methods (3) and (4) for most scenarios. This is because methods (1) and (2) assume symmetrical tower structures. The fault location errors of methods (1) and (2) become even larger with higher fault resistances. Although the multi-section π line model in method (3) is a good approximation of fully distributed parameter line model, the line model in matrix form PDE is the original fully distributed parameter model and is more accurate. The error of method (3) is caused by frequency dependency of line parameters; the

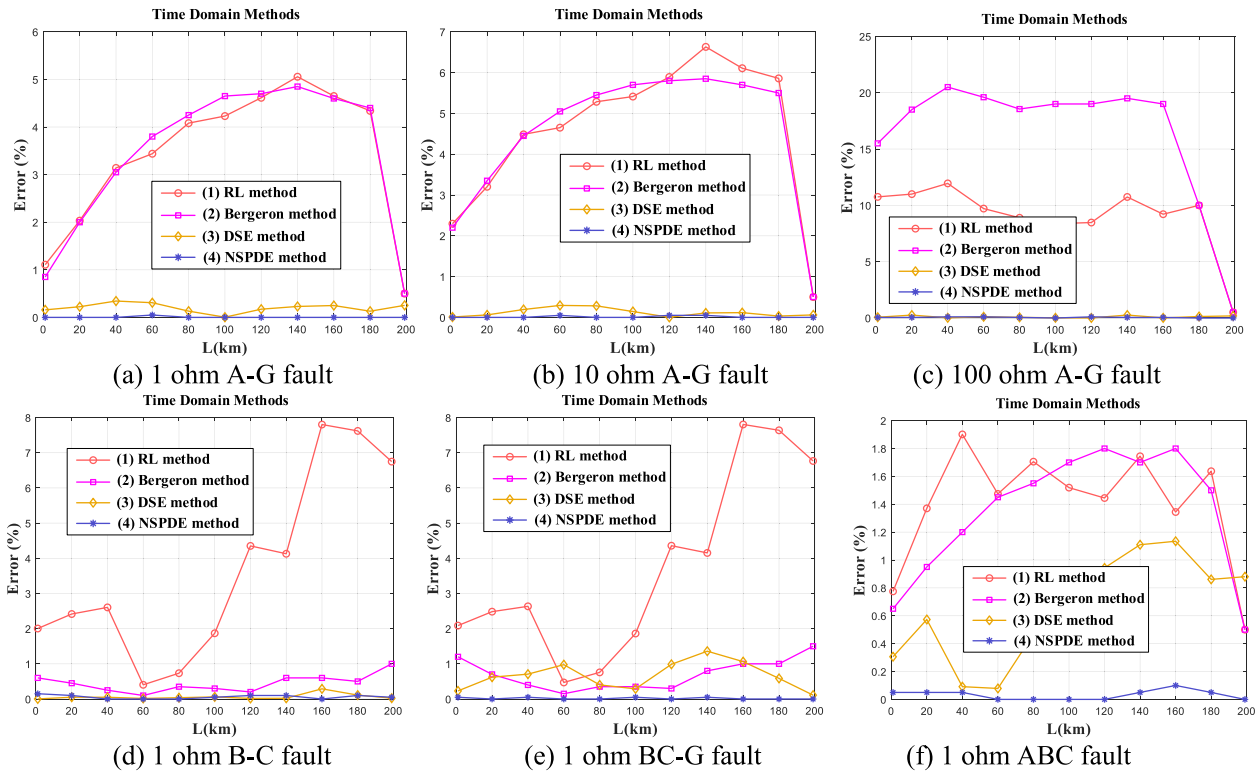


Fig. 27. Fault location results comparison, various time domain fault location approaches.

Table 5

Average and maximum errors, various time domain fault location approaches.

Fault location methods	A-G 1 Ω Faults		A-G 10 Ω Faults		A-G 100 Ω Faults	
	Averageerror (%)	Maxerror (%)	Averageerror (%)	Maxerror (%)	Averageerror (%)	Maxerror (%)
(1) RL method	3.3811	5.0565	4.5750	6.6310	9.0555	11.9494
(2) Bergeron method	3.4227	4.8500	4.5045	5.8500	16.3318	20.5000
(3) DSE method	0.2004	0.3438	0.1186	0.2934	0.1007	0.2608
(4) NSPDE method	0.0045	0.0500	0.0136	0.0500	0.0500	0.1000
Fault location methods	B-C 1 Ω Faults		BC-G 1 Ω Faults		ABC 1 Ω Faults	
	Averageerror (%)	Maxerror (%)	Averageerror (%)	Maxerror (%)	Averageerror (%)	Maxerror (%)
(1) RL method	3.6980	7.8012	3.7281	7.8031	1.4013	1.9010
(2) Bergeron method	0.4500	1.0000	0.7045	1.5000	1.3455	1.8000
(3) DSE method	0.0616	0.1500	0.6661	1.3588	0.6295	1.1346
(4) NSPDE method	0.0591	0.2890	0.0182	0.0500	0.0318	0.1000

method (4) is less affected by frequency dependent parameters since it can utilize the approximate “aerial mode” (or “line mode”) component for fault location.

In fact, one can compare the time domain fault location methods in Fig. 27 to the phasor domain methods in Fig. 26. It can be seen that, with similar lumped R-L line models, the fault location errors of time domain method (1) are larger than those of phasor domain method (1). This is also intuitive since the lumped RL model is more accurate for smaller frequency of interest: phasor domain methods focus on fundamental frequency components, while time domain methods adopt waveforms within a large range of frequencies (including high frequencies). Nevertheless, the key limitation for phasor domain methods is that they need a relatively long time window for accurate extraction of phasors. For time domain methods, only 10 ms (or even shorter) data window after the occurrence of the fault is required to obtain quite accurate fault location results.

5. Visions for future developments

5.1. Complex topologies of transmission lines

This paper primarily focuses on modeling of two-terminal homogeneous transmission lines and applying those line models to fault location on two-terminal homogeneous lines. In practical systems, there are still topologies other than two-terminal homogeneous lines, such as non-homogeneous lines (underground cables connected to overhead lines, overhead lines with different tower structures, etc.), parallel lines sharing the same tower or same right of way, three- or multi-terminal lines (measurements are only available at line terminals). In those cases, model-based fault location methods can be similarly applied. The key idea is to build the transmission line model for the entire system, introduce available measurements, and solve for the unknown fault location [28,58–59]. Also, faulted line segment identification approaches should be carefully investigated for transmission lines with complex topologies.

5.2. Modeling of fault arc

The location of the fault can also include phenomena related to fault arc, existing at the fault point. Such an arc is considered as a long arc in free air and its nature is purely resistive, introducing additional challenges when deriving highly accurate fault location algorithms, both in phasor and time domains. One of the first results published on this topic was presented in [69]. Here a phasor domain approach for determining the fault nature (arcing, or non-arcing fault) is presented. It can be used for blocking autoreclosure sequence in cases of non-arcing faults. Research results on understanding the fault nature and modeling this complex non-linear phenomena [70–73] have led to new phasor and time domain fault location algorithms not sensitive to voltage drop across the arc, particularly evident in cases in which the fault is fed from both line sides. Next to abovementioned time domain algorithms ([63]–[68]), the following phasor domain algorithms can be mentioned [74–76]. The arc model presented in [77] can be used for arcing faults modelling purposes and testing of fault location algorithms.

5.3. Fault location with high penetration of renewables

Power systems evolve with high penetration of renewables. Renewables are typically connected to the power system via converters. Fault characteristics of converter interfaced generations (CIGs) are very different from those of traditional synchronous machines: CIGs have much less inertia and therefore the transients are more severe during faults. In addition, the output currents of CIGs are limited to protect power electronics devices, and the equivalent source models of CIGs are dependent on their control strategies during faults. Therefore, the applicability of model-based fault location schemes should be carefully evaluated under those scenarios. On one hand, accurate transient and steady state modeling of CIGs during faults is essential to accurately describe the source characteristics and to enable accurate fault location. On the other hand, accurate time domain line modeling is also mandatory to ensure accuracy of model-based fault location methods, since severe transients could greatly increase the modeling error of transmission line and the fault location error.

5.4. Consideration of line frequency dependent parameters

As mentioned in section 2.1, the transmission line parameters are frequency dependent, i.e., the values of series resistance/inductance and shunt conductance/capacitance depend on the frequency of the voltage/current waveforms. In most fault location literatures, the line models are based on frequency independent (constant) parameters for simplification, as explained from section 2.2 to section 2.9. In fact, for phasor domain methods, the frequency dependent line parameters do not have much impact, since the frequency of the system is set as the fundamental frequency and the all the parameters are constants evaluated at the fundamental frequency. For time domain methods, since the waveforms include information within a wide frequency range, frequency dependent parameters are suggested to be considered to ensure the best performance of time domain model-based line fault location approaches.

There are several ways to consider/mitigate the impact of frequency dependent line parameters. For overhead lines, one can use “line mode” components or high frequency components to design the fault location algorithm. This is because the variation of line parameters with different frequencies become less for “line mode” or high frequency components [41,60]. For application where “ground mode” (“zero mode”) component needs to be utilized or the waveform intensity of high frequency components is not adequate, frequency dependent parameters should still be carefully considered. Moreover, frequency dependent characteristics become more severe for underground cables. In those cases, researchers also proposed methods to separate the phase conductors/soils into several layers, to well approximate the frequency dependent characteristics [44,61]. With severe and unusual transients in future

power systems with high penetration of renewables, accurate modeling of frequency dependent line parameters is still an important topic to be investigated, to enable accurate descriptions of line physical laws and design of different fault related applications such as fault location, protection and controls.

5.5. Identification of line parameters

Accurate model-based fault location methods require accurate transmission line parameters. However, in practice, accurate line parameters may not be available in the database. One solution is to present parameter identification approaches during normal operation of the system, to fine-tune those line parameters [62]. However, some parameters such as zero sequence parameters cannot be identified during normal operations. In those cases, with measurements before and during the fault, researchers proposed methods that can estimate fault location together with unknown line parameters, or parameter-free fault location methods [22–24,29–30,39,59]. The key idea is to use the redundant information before and during the fault to eliminate the impact of line parameters. Those methods still need further investigations in the future.

5.6. Combination of data and physics information for fault location

Data driven methods are attracting increasing attention in recent years due to its successful applications on computer vision, natural language processing, to name a few. Data driven methods for fault location have been proposed in the existing literatures [11–18]. However, fault location problems have their own challenges if data driven approaches are applied. First, fault related field data are not as many as data during normal operation, i.e., the field data are not quite representative, limiting the effectiveness of data driven approaches. Second, if simulation data are utilized for training, the gap between simulation data and field data needs to be well considered. Therefore, proper combinations of physics information and data driven approaches could be promising solutions to accurate fault location in practical power systems.

5.7. Accurate modeling of measurement chain

Model-based line fault location methods depend on accurate modeling of physical laws at the primary side of the power system. In practice, primary side voltages and currents may not be directly accessible. In this case, voltage and current transducers (DC systems) or instrumentation transformers (AC systems) are typically required. However, those transducers or instrumentation transformers could bring systematic errors to the measurements, which could affect the accuracy of fault location. For example, during saturation of current transformers (CTs), the primary side current and secondary side current does not follow the relationship of transformer ratio. Also, the coupling capacitor voltage transformers (CCVTs) could also suffer from waveform distortions during transients. In addition, the extraction of phasor measurements from instantaneous measurements could also generate errors. In those cases, accurate modeling of the measurement chain is required, to accurately recover primary side voltages and currents for fault location.

5.8. High fidelity line models for AI/ML-based fault location methods

Methods based on Artificial Intelligence (AI) and Machine Learning (ML) require high fidelity physical system model for their training and design. In this paper, adequate line model can support the training procedure and consequently the efficacy of AI/ML-based methods.

6. Conclusions

This paper systematically reviews the model-based transmission line

fault location methods. First, the overall transmission line modeling procedure for fault location is summarized, and various time domain and phasor domain transmission line models are presented. The relationship between different modeling approaches, as well as the assumptions for each modeling method are carefully demonstrated. Afterwards, with different transmission line models, phasor domain and time domain model-based fault location approaches are shown in detail, to demonstrate how to establish fault location problem and determine fault location using various transmission line models. Furthermore, the performances of model-based fault location methods with different line models are compared via numerical experiments. The results clearly indicate the importance to use accurate transmission line models for fault location. The results also show that, compared to phasor domain methods, time domain model-based fault location methods can accurately locate faults with a short data window after the fault occurs. Views for future developments are also discussed.

Declaration of Competing Interest

The authors declare that they have no known competing financial interests or personal relationships that could have appeared to influence the work reported in this paper.

Data availability

The authors do not have permission to share data.

Acknowledgements

This work is supported by National Natural Science Foundation of China (No. 51807119) and Key Laboratory of Control of Power Transmission and Conversion (SJTU), Ministry of Education (No. 2022AB01). Their support is greatly appreciated. The authors would also like to thank Ms. Yiqi Xing, Mr. Yuan Nie and Mr. Mengzhao Duan from School of Information Science and Technology, ShanghaiTech University for their valuable contributions. Work of Vladimir Terzija and Stepan Vasilev is supported by Skoltech and The Ministry of Education and Science of Russian Federation, Grant Agreement No 075-10-2021-067, Grant identification code 000000S707521QJX0002.

References

- Lotfjou A, Fu Y, Shahidehpour M. Hybrid AC/DC transmission expansion planning. *IEEE Trans Power Syst* 2012;27(3):1620–8.
- Wang B, Liu Y, Yue K, Lu D, Zhao J. Improved dynamic state estimation based protection on transmission lines in MMC-HVDC grids. *IEEE Trans Power Del* 2022;37(5):3567–81.
- Kezunovic M. Smart fault location for smart grids. *IEEE Trans Smart Grid* 2011;2(1):11–22.
- Magnago FH, Abur A. Fault location using wavelets. *IEEE Trans Power Del* 1998;13(4):1475–80.
- Jia Y, Liu Yu, Wang B, Lu D, Lin Y. Power network fault location with exact distributed parameter line model and sparse estimation. *Electric Power Syst Res* 2022;212:108137.
- IEEE Standard C37.114. *IEEE Guide for Determining Fault Location on AC Transmission and Distribution Lines*; 2014.
- Abd el-Ghany HA, Azmy AM, Abeid AM. A general travelling-wave-based scheme for locating simultaneous faults in transmission lines. *IEEE Trans Power Del*, Feb 2020;35(1):130–9.
- Qiao J, et al. A multi-terminal traveling wave fault location method for active distribution network based on residual clustering. *Int J Electr Power Energy Syst* 2021;131:107070.
- Reis RLA, et al. An improved single-ended correlation-based fault location technique using traveling waves. *Int J Electr Power Energy Syst* 2021;132:107167.
- Xu Y, Liu Y, Xing Y, Nie Y, Huang W. Power network fault location using traveling waves and continuous wavelet transform. *IEEE Power Energy Soc General Meeting Jul*. 2022:1–5.
- Farshad M, Sadeh J. Accurate single-phase fault-location method for transmission lines based on K-nearest neighbour algorithm using one-end voltage. *IEEE Trans Power Del* Oct. 2012;27(4):2360–7.
- Livani H, Evrenosoglu CY. A machine learning and wavelet based fault location method for hybrid transmission lines. *IEEE Trans Smart, Grid* 2013;5(1):51–9.
- Swetapadma A, Yadav A. A novel decision tree regression-based fault distance estimation scheme for transmission lines. *IEEE Trans Power Del* 2017;32(1):234–45.
- Gracia J, Mazon AJ, Zamora I. Best ANN structures for fault location in single- and double-circuit transmission lines. *IEEE Trans Power Del* 2005;20:2389–95.
- Tsotsopoulou E, et al. Advanced fault location scheme for superconducting cables based on deep learning algorithms. *Int J Electr Power Energy Syst* 2023;147:108860.
- Chen K, Hu J, Zhang Y, Yu Z, He J. Fault location in power distribution systems via deep graph convolutional networks. *IEEE J Sel Areas Commun* 2020;38(1):119–31.
- Xing Y, Liu Y, Wang B, Yi L, He X. Physics-informed data-driven transmission line fault location based on dynamic state estimation. *IEEE Power Energy Soc General Meeting* 2022:1–5.
- Xing Y, Liu Y, Nie Y, Li R, He X. Data-driven transmission line fault location with knowledge-aware graph neural network. *IEEE Power Energy Soc General Meeting* 2022:1–5.
- IEC Standard 61850, "Communication networks and systems in substations," 2003.
- IEEE Standard C37.111. *Common Format for Transient Data Exchange (COMTRADE) for Power Systems*; 1999.
- Apostolopoulos C, Korres GN. A novel algorithm for locating faults on transposed/untransposed transmission lines without utilizing line parameters. *IEEE Trans Power Del* 2010;25(4):2328–38.
- Preston G, Radojevic Z, Kim CH, Terzija V. New settings-free fault location algorithm based on synchronised sampling. *IET Gener Transmiss Distrib* 2011;5(3):376–83.
- Dobakhshari AS. Noniterative parameter-free fault location on untransposed single-circuit transmission lines. *IEEE Trans Power Del* 2017;32(3):1636–44.
- Lu D, Liu Y, Chen S, Wang B, Lu D. An improved noniterative parameter-free fault location method on untransposed transmission lines using multi-section models. *IEEE Trans Power Del* 2022;37(3):1356–69.
- Izykowski J, Rosolowski E, Balcerek P, Fulczyk M, Saha MM. Accurate noniterative fault-location algorithm utilizing two-end unsynchronized measurements. *IEEE Trans Power Del* 2011;26(2):547–55.
- Azizi S, Sanaye-Pasand M, Paolone M. Locating faults on untransposed, meshed transmission networks using a limited number of synchrophasor measurements. *IEEE Trans Power Syst* 2016;31(6):4462–72.
- Jiao X, Liao Y. Accurate fault location for untransposed/Transposed transmission lines using sparse wide-area measurements. *IEEE Trans Power Del* 2016;31(4):1797–805.
- Liu Y, et al. Fault location algorithm for non-homogeneous transmission lines considering line asymmetry. *IEEE Trans Power Del* 2020;35(5):2425–37.
- Kalita K, Anand S, Parida SK. A closed form solution for line parameter-less fault location with unsynchronized measurements. *IEEE Trans Power Del* 2022;37(3):1997–2006.
- Lu D, Liu Yu, Lu D, Wang B, Zheng X. Unsynchronized fault location on untransposed transmission lines with fully distributed parameter model considering line parameter uncertainties. *Electric Power Syst Res* 2022;202:108137.
- IEEE Standard C37.118. *IEEE Standard for Synchrophasor Data Transfer for Power Systems*; 2011.
- Kumar BR, Kumar A. Mitigation of the DC offset by a SubCycle sample method M-class PMUs. *IEEE Trans Power Del* 2019;34(2):780–3.
- Lu D, Liu Y, Wang B, Xing Y. Generalized phasor estimation method based on DFT with DC offset mitigation. *IEEE Power Energy Soc General Meeting* 2021:1–5.
- Xu J, Lv Y, Zhao C, Liang J. A model-based DC fault location scheme for multi-terminal MMC-HVDC systems using a simplified transmission line representation. *IEEE Trans Power Del* 2020;35(1):386–95.
- Liu Y, Meliopoulos AP, Tan Z, Sun L, Fan R. Dynamic state estimation-based fault locating on transmission lines. *IET Gener Transm Distrib* 2017;11(17):4184–92.
- Wang B, Liu Y, Lu D, Yue K, Fan R. Transmission line fault location in MMC-HVDC grids based on dynamic state estimation and gradient descent. *IEEE Trans Power Del* 2021;36(3):1714–25.
- Liu Y, et al. Dynamic state estimation for power system control and protection. *IEEE Trans Power Syst* 2021;36(6):5909–21.
- Suonan J, Gao S, Song G, Jiao Z, Kang X. A novel fault-location method for HVDC transmission lines. *IEEE Trans Power Del* 2010;25(2):1203–9.
- Liang Y, Wang G, Li H. Time-domain fault-location method on HVDC transmission lines under unsynchronized two-end measurement and uncertain line parameters. *IEEE Trans Power Del Jun*. 2015;30(3):1031–8.
- Lu D, Liu Y, Huang W, Xi X. Accurate fault location in AC/DC hybrid line corridors based on eigenvalue decomposition. *IEEE Power Energy Soc General Meeting* 2020:1–5.
- Yi L, Liu Y, Lu D, Nie Y, Zheng X. HVDC line fault location using wavelets to mitigate impact of frequency dependent line parameters. *IEEE Power Energy Soc General Meeting* 2022:1–5.
- Gopalakrishnan A, Kezunovic M, McKenna SM, Hamai DM. Fault location using the distributed parameter transmission line model. *IEEE Trans Power Del* 2000;15(4):1169–74.
- Lu D, Liu Y, Liao Q, Wang B, Huang W, Xi X. Time-domain transmission line fault location method with full consideration of distributed parameters and line asymmetry. *IEEE Trans Power Del Dec*. 2020;35(6):2651–62.
- Lu D, Liu Y, Xie J, Wang B, Liao Q. Multi-layer model enabled fault location for underground cables in MMC-HVDC grids considering distributed and frequency dependent line parameters. *IEEE Trans Power Del Aug*. 2022;37(4):3082–96.

- [45] Qiu J, Liu Y, Lu D, Nie Y, Liu Z. General format of phase-mode transformation matrices for 3 phase power systems and applications to transmission line protection. *IEEE Innovative Smart Grid Technologies (ISGT) Asia*, Oct 2022.
- [46] Das S, Santoso S, Gaikwad A, Patel M. Impedance-based fault location in transmission networks: theory and application. *IEEE Access* 2014;2:537–57.
- [47] Takagi T, Yamakoshi Y, Yamaura M, Kondow R, Matsushima T. Development of a new type fault locator using the one-terminal voltage and current data. *IEEE Trans Power Appar Syst PAS-101*, no. 8, pp. 2892–2898, Aug. 1982.
- [48] Lopes FV, Leite Jr EJS, Ribeiro JPG, Piardi AB, Scheid AV, Zat G, et al. Single-ended multi-method phasor-based approach for optimized fault location on transmission lines. *Electric Power Syst Research* 2022;212:108361.
- [49] Eriksson L, Saha MM, Rockefeller GD. An accurate fault locator with compensation for apparent reactance in the fault resistance resulting from remote-end infeed. *IEEE Trans Power Appar Syst* 1985;PER-5(2):44.
- [50] Chang P, Song G, Hou J, Xu R. A Single-terminal fault location method for transmission lines integrated by inverter-type source. *IEEE Trans Power Del Jun*. 2022;37(3):1704–13.
- [51] Zhang C, Song G, Yang L, Sun Z. Time-domain single-ended fault location method that does not need remote-end system information. *IET Gener Transm Distrib Nov*. 2019;2(14):284–93.
- [52] He Z-Y, Liao K, Li X-P, Lin S, Yang J-W, Mai R-K. Natural frequency-based line fault location in HVDC lines. *IEEE Trans Power Del* 2014;29(2):851–9.
- [53] Song G, Chu Xu, Cai X, Gao S, Ran M. A fault-location method for VSC-HVDC transmission lines based on natural frequency of current. *Int J Electr Power Energy Syst* 2014;63:347–52.
- [54] He J, Li B, Sun Q, Li Ye, Lyu H, Wang W, et al. The improved fault location method based on natural frequency in MMC-HVDC grid by combining FFT and MUSIC algorithms. *Int J Electr Power Energy Syst* 2022;137:107816.
- [55] Nie Y, et al. An improved natural frequency based transmission line fault location method with full utilization of frequency spectrum information. *IET Gener Transm Distrib Oct* 2021;15(19):2787–803.
- [56] Meliopoulos APS, Cokkinides GJ, Myrda P, Liu Yu, Fan R, Sun L, et al. Dynamic state estimation based protection: status and promise. *IEEE Trans Power Del* 2017; 32(1):320–30.
- [57] Liu Y, Meliopoulos AP, Fan R, Sun L, Tan Z. Dynamic state estimation based protection on series compensated transmission lines. *IEEE Trans Power Del Oct*. 2017;32(5):2199–209.
- [58] Lee Y, Lin T, Liu C. Multi-terminal nonhomogeneous transmission line fault location utilizing synchronized data. *IEEE Trans Power Del Jun*. 2019;34(3): 1030–8.
- [59] Wang B, Liu Yu, Lu D, Yue K, Nie Y. Unsynchronized parameter-free fault location for two or three terminal double-circuit transmission lines sharing the same tower via unscented Kalman filter. *IEEE Trans Power Del* 2023;38(3):1731–46.
- [60] Li B, et al. An improved transient traveling-wave based direction criterion for multi-terminal HVDC grid. *IEEE Trans Power Del* 2020;35(5):2517–29.
- [61] Xie J, Meliopoulos AP, Liu Y. Low broadband transmission line model for geomagnetically induced current analysis. *IEEE Power Energy Soc General Meeting*; 2018. pp. 1-5.
- [62] Varghese AC, Pal A, Dasarathy G. Transmission line parameter estimation under non-gaussian measurement noise. *IEEE Trans Power Syst* 2022.
- [63] Djuric MB, Radojevic ZM, Terzija VV. Time domain solution of fault distance estimation and arcing faults detection on overhead lines. *IEEE Trans Power Del Jan*. 1999;14(1):60–7.
- [64] Djurić MB, Terzija VV, Radojević ZM. Overhead lines fault location and arc voltage estimation numerical algorithm derived in time domain. *Lichtbogen Spannung und Fehlerdistanz Schätzung in Freileitungsnetzen mittels im Zeitbereich entwickelten numerischen Algorithmus*. *Electr Eng* 1998;81(1):45–53.
- [65] Djuric MB, Radojevic ZM, Terzija VV. On time domain overhead lines numerical protection. *Electric Mach Power Syst* 1999;27(8):889–904.
- [66] Radojevic ZM, Terzija VV, Djuric NB. Numerical algorithm for overhead lines arcing faults detection and distance and directional protection. *IEEE Trans Power Del Jan*. 2000;15(1):31–7.
- [67] Terzija VV, Radojevic ZM. Numerical algorithm for adaptive autoreclosure and protection of medium-voltage overhead lines. *IEEE Trans Power Del* 2004;19(2): 554–9.
- [68] Terzija V, Preston G, Stanojević V, Elkalashy NI, Popov M. Synchronized measurements-based algorithm for short transmission line fault analysis. *IEEE Trans Smart Grid Nov*. 2015;6(6):2639–48.
- [69] Djurić M, Terzija V. A new approach to the arcing faults detection for fast autoreclosure in transmission systems. *IEEE Trans Power Del Oct*. 1995;10(4): 1793–8.
- [70] Terzija V, Koglin H-J. On the modeling of long arc in still air and arc resistance calculation. *IEEE Trans Power Del* 2004;19(3):1012–7.
- [71] Terzija VV, Koglin HJ. Long arc in free air: laboratory testing, modelling, simulation and model-parameters estimation. *Generat Trans Distrib IEE Proceedings May* 2002;149(3):319–25.
- [72] Terzija V, Koglin HJ. A new approach to arc resistance calculation. *Electr Eng, Archiv für Elektrotechnik* 2001;83(4):187–92.
- [73] Terzija V, Koglin H-J. New dynamic model, laboratory testing and features of long arc in free air. *Electr Eng, Archiv für Elektrotechnik* 2001;83(4):193–201.
- [74] Radojević Z, Terzija V, Preston G, Padmanabhan S, Novosel D. Smart overhead lines autoreclosure algorithm based on detailed fault analysis. *IEEE Trans Smart Grid* 2013;4(4):1829–38.
- [75] Radojevic Z, Terzija V. Numerical algorithm for overhead lines protection and disturbance records analysis. *IET Gener Transm Distrib March* 2007;1(2):357–63.
- [76] Terzija V, Radojevic Z. Numerical algorithm for adaptive autoreclosure and protection of medium voltage overhead lines. *IEEE Trans Power Del April* 2004;19 (2):554–9.
- [77] Terzija V, Preston G, Popov M, Terzija N. New static 'AirArc' EMTF model of long arc in free air. *IEEE Trans Power Del* 2011;26(99):1344–53.
- [78] Schweitzer EO, Guzman A, Mynam MV, Skendzic V, Kasztenny B, Marx S. Protective relays with traveling wave technology revolutionize fault locating. *IEEE Power Energy Mag* 2016;14(2):14–20.
- [79] Nguyen VN, Janssen R, Roverso D. Automatic autonomous vision-based power line inspection: a review of current status and the potential role of deep learning. *Int J Electr Power Energy Syst* 2018;99:107–20.
- [80] Ge Y. *New protective relaying and fault location: principles and techniques* (2nd edition). Xi'an Jiao Tong University Press: Xi'an, China; 2007 (in Chinese).